UNIVERSITY OF
EASTERN FINLAND

EVALUATING THE ROLE OF PREADIPOCYTES IN TISSUE REMODELING ASSOCIATED WITH ATHEROSCLEROSIS

Jade Liikkanen
Master of Science thesis
Master's Degree Programme in Biomedicine
University of Eastern Finland
Faculty of Health Sciences
School of Medicine
16.4.2021

University of Eastern Finland, Faculty of Health Sciences, School of Medicine
Master's Degree Programme in Biomedicine
Jade Liikkanen: Evaluating the role of preadipocytes in tissue remodeling associated with atherosclerosis
Master of Science thesis; 43 pages, 10 appendixes
Supervisors: Minna Kaikkonen-Määttä, Associate professor; Uma Thanigai Arasu, Ph.D.
16.4.2021

Keywords: adipose tissue, extracellular matrix, preadipocyte, adipocyte, atherosclerosis

Abstract

Expanding adipose tissue upon obesity induces remodeling of the surround extracellular matrix, a process in which preadipocytes are exposed to pro-inflammatory conditions. In addition, remodeling of the extracellular matrix takes place in the atherosclerotic lesions but only limited number of studies investigating the role of preadipocytes in atherosclerosis exists. Our preliminary data from *in vivo* mouse model showed an increased fibrotic activity of mesenchymal stem cells in adipose tissue when the mice were subjected to high-fat diet for 3 months. In the present study, human Simpson-Golabi-Behmel syndrome (SGBS) preadipocytes were treated with ligands predicted to be involved in the obesogenic and atherogenic environment. In addition, we silenced *SERPINE1*, a gene involved in the atherogenesis. Using high-throughput RNA sequencing, we validated the expression of genes in SGBS preadipocytes that were expressed in our preliminary data and identified differentially expressed genes in SGBS cells in response to the treatments. We found several genes related to adipogenesis, extracellular matrix, and atherosclerosis differentially expressed. In response to the obesogenic/atherogenic factors, the AGE-RAGE signaling pathway associated with atherosclerosis was enriched. Collectively, these results suggest that preadipocytes might be one potential contributor to the progression of atherosclerosis, either directly through the AGE-RAGE signaling pathway or paracrine signaling, or indirectly via adipogenesis and remodeling of the extracellular matrix. Hence, their adipogenic and extracellular matrix remodeling potential, as well as interaction with other cell types, may provide new insights into understanding the obesity-related cardiovascular diseases.

Introduction

Adipose tissue is known to affect cardiovascular health and disease. Healthy adipose tissue is important for metabolic homeostasis, as it has an endocrine function and can affect many organs in either autocrine, paracrine, and/or endocrine way. However, when adipose tissue turns dysfunctional, it acts as a contributing factor to metabolic disease pathogenesis. For example, an excessive caloric intake and the subsequent obesity causes lipid accumulation in adipocytes, adipose tissue inflammation, fibrosis, and oxidative stress, all of which promote metabolic dysfunction and can predispose to the development of cardiovascular diseases (CVD; Ha & Bauer, 2018; Oikonomou & Antoniades, 2019). Previously, our research group has discovered that a specific cell population, putatively preadipocytes, of visceral adipose tissue (VAT) from high-fat diet fed $LDLR^{-/-}/ApoB^{100/100}$ mice undergoes changes in their gene expression during the progression of atherosclerosis (unpublished results). More specifically, in the late stage of the disease, this cell population developed a pro-fibrotic phenotype characterized by increased expression of genes related to the organization and remodeling of the extracellular matrix (ECM) as well as to collagen biosynthesis and degradation. Hence, our findings suggested that this cell population undergoes a switch from the (pre)adipocytic features to the pro-fibrotic features under high-fat diet thus establishing a link between obesity, ECM remodeling, and atherosclerosis. As our preliminary data arise from mouse studies and differences in gene expression between species might exist, the aim of this thesis work was to validate genes whose expression has changed during the atherosclerosis progression *in vivo* using an experimental *in vitro* model of human preadipocytes. In addition, we investigated which ligands predicted to be present in the atherosclerotic environment could be responsible for the gene expression changes in preadipocytes, what are the reported functional roles of ECM remodeling genes in preadipocytes based on literature, and how does perturbation of selected candidate genes affect downstream gene expression.

The emerging knowledge of adipose tissue and its function in cardiovascular health has revealed that the biological profile of the adipose tissue widely depends on its expansion, body distribution, as well as the quality and differences in local biology. White adipose tissue (WAT), the predominant type of adipose tissue in the human body, is usually divided into two main anatomical depots, subcutaneous adipose tissue (SAT) and VAT (Oikonomou & Antoniades, 2019), among which particularly the visceral adiposity is associated with incident CVD (Britton et al, 2013). In addition, VAT can be further classified based on its anatomical location. For example, intrathoracic VAT can be divided into epicardial and perivascular adipose tissue (PVAT) which are important for cardiovascular risk (Ouwens et al, 2010). The majority of adipose tissue is composed of adipocytes responsible for energy

storage, although adipose tissue also contains, for example, inflammatory cells, fibroblasts, vascular cells, preadipocytes, and multipotent mesenchymal stem-like cells (Oikonomou & Antoniades, 2019). During obesity, adipose tissue expands through enlargement of individual adipocytes as they accumulate lipids (hypertrophy), or by forming of new adipocytes through differentiation of preadipocytes (hyperplasia, adipogenesis). In general, hypertrophic adipose expansion is associated with unfavorable outcomes as it is characterized by necrosis-like adipocyte death, increased expression and secretion of pro-inflammatory cytokines, local adipose tissue hypoxia, and elevated basal lipolysis. The latter leads to increased leakage of free fatty acids from adipose tissue which are taken up by other tissues, thus causing ectopic lipid accumulation. In contrast, hyperplastic adipose expansion can provide additional capacity to store lipids due to *de novo* differentiation of preadipocytes and therefore, ameliorate for example insulin resistance (Choe et al, 2016). Increasing fat mass induces a strong structural remodeling of the adipose tissue that is required to provide enough space for the enlargement of adipocytes, and to form new adipocytes (Ruiz-Ojeda et al, 2019). The remodeling contains alterations in the adipose tissue structure, size, and shape, as well as in the stromal part and ECM (Divoux & Clément, 2011). During the adipose expansion and remodeling, angiogenesis is required to ensure the accessibility of oxygen, nutrients, cytokines, and growth factors to the tissue (Corvera & Gealekman, 2014). If angiogenesis does not increase at a similar rate to that of WAT, it may result in tissue dysfunction and hypoxia, the latter of which has been assumed to be the major initiating factor for the ECM induction and fibrosis (Sun et al, 2013).

The adipose ECM, first observed by Napolitano et al in 1963, is a complex three-dimensional network that has an important role in the adipose tissue by providing structural and biochemical support to surrounding cells and the whole tissue. As both adipocytes and preadipocytes exist within the ECM network, ECM proteins are able to regulate the adipose tissue function through physical interactions (Chun, 2012). For example, the ECM can control cell proliferation, adhesion, migration, polarity, differentiation, and apoptosis. Additionally, it is a reservoir of growth factors and different bioactive molecules, such as fibroblast growth factor and transforming growth factor β (TGF-β; Yue, 2014). The ECM is composed of extracellular carbohydrate and protein components that are connected to the cells through different receptors, such as integrins, CD36, and CD44 (Ruiz-Ojeda et al, 2019; Yue, 2014). Due to broad ligand-binding specificities, integrins have the major role in the ECM-cell adhesion and signaling into the cells (Ruiz-Ojeda et al, 2019). Some of the integrin subunits have also been associated with obesity and insulin resistance (Lin et al, 2016; Ruiz-Ojeda et al, 2021). In turn, CD36 can bind several ligands, including collagen, thrombospondin, lipoproteins, and fatty acids, and it is involved in free fatty acid transportation into the adipose tissue (Lin et al, 2016). Unlike

integrins and CD36, CD44 functions as a receptor mainly for hyaluronan and osteopontin. The CD44 expression is positively correlated with adipose tissue inflammation and insulin resistance and thus, it has been suggested that osteopontin, also known as secreted phosphoprotein 1 (Spp1), could mediate macrophage infiltration and activation in adipose tissue and/or systemic insulin resistance through CD44 (Liu et al, 2015).

The most important components of ECM are collagens which also contribute to cell adhesion, migration, differentiation, morphogenesis, and wound healing. Both fibrillar (type I, III) and non-fibrillar (type IV, VI, VII) collagens are found in the adipose tissue ECM. For example, type I collagen is the most abundant component of the ECM, while type VI collagen is found in greater amounts in adipose tissue compared to other tissue types. In turn, type IV collagen together with laminin form a major part of the adipocytes' basement membrane and thus, they are necessary for adipocytes' survival. Although collagens are vital for the adipose ECM, their increased expression and deposition in obesity creates a physical barrier against adipocyte hypertrophy. This may further inhibit angiogenesis and predispose to tissue dysfunction and fibrosis (Lin et al, 2016; Ruiz-Ojeda et al, 2019). In addition to collagen, the ECM of adipose tissue contains glycoproteins, such as fibronectin, fibrillin, laminin, thrombospondin, and Spp1. Fibronectin is another major component of the ECM that, in addition to the regulation of tissue and ECM architecture, has been shown to inhibit adipogenesis and may contribute to obesity (Chun, 2012; Divoux & Clément, 2011; Lee et al, 2013). In turn, fibrillin is a component of ECM microfibrils that are required for elastic fiber formation and to provide structural elasticity for the tissue (Muthu & Reinhardt, 2020), whereas Spp1 is an ECM glycoprotein and pro-inflammatory cytokine which deficiency has shown to attenuate the development of atherosclerosis in mice (Matsui et al, 2003). Besides Spp1, thrombospondin is another ECM component with pro-inflammatory properties (Divoux & Clément, 2011). It can also interact with a variety of ECM components, among which the interaction with type V collagen has been assumed to be a biological modifier of adipocyte function (Chun, 2012).

In the ECM remodeling, matrix metalloproteinases (MMPs) and tissue inhibitor of metalloproteinases (TIMPs) are enzymes responsible for the deposition, degradation, and modification of the ECM components (Ruiz-Ojeda et al, 2019). As the remodeling of the ECM takes place not only in the adipose tissue but also in the vasculature and atherosclerotic plaques, the local balance of MMP and TIMP activity is important for maintaining healthy conditions, as well as for the progression of atherosclerosis (Galis & Khatri, 2002). In addition, remodeling of the ECM during obesity has a major role in the development of adipose tissue fibrosis, characterized by an accumulation of ECM components, particularly insoluble collagen fibrils, fibronectin, and elastin (Halberg et al, 2009).

Although the obesity-associated adipose tissue fibrosis is well characterized, its metabolic outcomes are controversial. One assumption is that excess deposition of collagen or ECM leads to loss of ECM flexibility and provide shear stress to expanding adipocytes, resulting in adipocyte death and inflammation. On the other hand, ECM deposition may limit the excessive growth of adipocytes and therefore, lead to reduced adipocyte hypertrophy (Datta et al, 2018). In the former case, decreased ECM flexibility may hinder adipocyte expansion and lead to lipid accumulation into other tissues (Suganami et al, 2012), such as skeletal muscle, liver or blood vessels, and predispose to insulin resistance or CVD.

As preadipocytes express the majority of ECM components, they are assumed to play a role in the ECM production and the adipose tissue fibrosis (Datta et al, 2018). Moreover, Keophiphath et al (2009) have shown that preadipocytes accumulate in the fibrotic areas within WAT of obese individuals, and preadipocytes can acquire pro-inflammatory properties in the presence of inflammatory stimuli. When stimulated with macrophage-secreted factors, inflammatory preadipocytes have shown highly ordered and abundant synthesis of ECM components, including type I collagen and fibronectin (Henegar et al, 2008; Keophiphath et al, 2009). Although adipocyte progenitors consist of multiple subsets with different functional roles (Raajendiran et al, 2019), PDGFRα^+ preadipocytes, as characterized also in our study, can adopt a myofibroblast-like phenotype during obesity. Marcelin et al (2017) have shown that PDGFRα^+ preadipocytes are a source of fibrotic components and pro-inflammatory factors and therefore, obesity and adipose fibrosis seems to affect preadipocytes' adipogenic capacity and limit the adipose lipid uptake following ECM deposition (Marcelin et al, 2017). In addition to preadipocytes, dedifferentiation of mature adipocytes into fibroblast-like cells has been characterized. They have also been shown to express both pro-inflammatory factors and genes associated with the ECM remodeling (Lessard et al, 2015). Altogether, ECM has an extensive influence on the adipose tissue biology, and it is "a ripe area both for mechanistic investigative research and for therapeutic drug development" as concluded in the review of Datta et al (2018).

Besides fibrosis, inflammation plays an important role in the obese adipose tissue, as the hypertrophic adipocytes cause hypoxia that leads to adipocyte death and attracts macrophages. Communication between adipose tissue and immune cells is bi-directional, as the activated immune cells secrete pro-inflammatory cytokines that affect adipocytes' function, differentiation, and adipokine secretion, further promoting the inflammatory state itself (Guzik et al, 2017). Moreover, inflammation and fibrosis are partly connected, as discussed in the review of Datta et al (2018). Although the

relationship between fibrosis and inflammation is complex, both are suggested to form a link between obesity and CVD (Chun, 2012). In example, Carrol & Tyagi (2005) have demonstrated that obesity and high-fat intake induce cardiovascular fibrosis and hypertrophy in rabbits by increasing collagen and TGF-β expression (Carrol & Tyagi, 2005). Obesity is also associated with arterial stiffness that is partly mediated by ECM remodeling, adipocyte-derived factors, as well as by immune and inflammatory responses. Especially PVAT, that in normal conditions have cardioprotective effects, loses its vascular protective effect in obesity, and can therefore contribute to vascular stiffness and CVD (Aroor et al, 2018). In turn, the review of León-Pedroza et al (2015) shows that obesity is associated with not only local but also systemic inflammation that is an important contributor to CVD (León-Pedroza et al, 2015). Particularly VAT is able to secrete varying pro-inflammatory factors that are linked to the development of atherosclerosis and/or other CVD (Berg & Scherer, 2005). Taken together, obesity is an independent risk factor for CVD as it promotes tissue fibrosis through ECM accumulation and remodeling (Buechler et al, 2015) and reduces the ability of preadipocytes to differentiate into mature adipocytes and store lipids, thus promoting ectopic lipid deposition (Gustafson & Smith, 2006). Furthermore, obesity causes changes in the adipokine secretion (Zorena et al, 2020), promotes systemic low-grade inflammation through secretion of pro-inflammatory factors from enlarged adipocytes that further attracts macrophages in adipose tissue (León-Pedroza et al, 2015), and predisposes to insulin resistance and dyslipidemia (Libby et al, 2002).

In atherosclerosis, lipids, inflammatory cells, and ECM accumulate into the vessel wall (Libby et al, 2002). The atherosclerotic plaques consist of a lipid core covered by a thin fibrous cap in which large amounts of ECM are deposited. Among the ECM components, collagen makes up to 60 % of the total protein content of the fibrous cap, and the collagen content increases in parallel with plaque formation and progression. In addition to collagen, elastin, glycoproteins i.e., fibronectin, thrombospondin-1 (THBS1), and Spp1, as well as proteoglycans are included in the plaque formation (Katsuda & Kaji, 2003). Vascular smooth muscle cells are considered to be responsible for the ECM production in the atherosclerotic plaques, although also fibroblasts and myofibroblasts of the vascular adventitia can participate in the neo-intima formation (Sartore et al, 2001). This raises questions whether (pre)adipocytes, that are also located in the vascular adventitia and able to adopt the myofibroblast-like phenotype, could also participate in the plaque formation. In any case, the excess deposition of the ECM in the cap makes the outer layer more strength, whereas enhanced ECM degradation in the lipid core makes the plaque more fragile and vulnerable to rupture (Katsuda & Kaji, 2003). Like in the adipose tissue, remodeling of the ECM in the atherosclerotic lesions is carried out by MMPs and TIMPs, although the outcome of MMP activity is not clear. On one hand, increased MMP activity

can promote the plaque rupture as it degrades collagen in the cap, whereas on the other hand, inhibition of the MMP activity may also lead to progression of atherosclerosis as it allows the excess ECM deposition (Heeneman et al, 2003).

Despite obesity and adipose biology playing an important role in CVD, there are only a limited number of studies investigating the relationship between preadipocytes and atherosclerosis. Altogether, a few studies indicate that preadipocytes of PVAT are likely to affect the development of CVD. Rittig et al (2012) have shown that PVAT preadipocytes exhibit a higher level of angiogenic, growth stimulatory, inflammatory, and metabolic factors compared to preadipocytes of subcutaneous or visceral fat (Rittig et al, 2012). Moreover, secretion of pro-inflammatory cytokines and chemokines are higher in preadipocytes than mature adipocytes of PVAT (Berti et al, 2016). In the study of Parvizi et al (2021), endothelial cells, smooth muscle cells, and macrophages induced an inflammatory phenotype when cultured with inflammatory/senescent preadipocytes. Additionally, the studied vascular cells demonstrated decreased viability, disrupted proliferation and migration, and impaired metabolic function. Thus, they suggest that senescent preadipocytes in PVAT or in close proximity to blood vessels can trigger phenotypic and functional changes in the cellular components of vasculature, therefore possibly contributing to vascular disease (Parvizi et al, 2021). Finally, the communication between the adipose tissue and vasculature seems to be bi-directional, as the inflammatory mediators produced in the vascular wall are able to inhibit the differentiation of PVAT preadipocytes, and reduce their lipid accumulation through paracrine signaling *in vitro*, *ex vivo*, and *in vivo* (Antonopoulos et al, 2017). Hence, understanding the (pre)adipocyte function and development are required for understanding the alterations in adiposity and its direct links to morbidity, mortality, and many disorders. Additionally, not much are known about the role of preadipocytes in ECM remodeling associated with atherosclerosis, or the specific changes in the atherosclerotic environment that drive preadipocytes into disease-promoting phenotype. Thus, studies within human preadipocytes could provide an important information about their contribution to ECM remodeling in both obesity and atherosclerosis progression.

Here, using an experimental *in vitro* model of human Simpson-Golabi-Behmel syndrome (SGBS) preadipocytes, we validated the expression of 38 genes that were differentially expressed during the atherosclerosis progression *in vivo*. Importantly, these genes were predicted to be regulated by TGF-β1, IL-1β, angiotensin II (Agt II), or Spp1 ligands. In addition, we showed that stimulation of preadipocytes with the above-mentioned factors contributing to the atherosclerotic environment induces the expression of genes related to atherogenesis, adipogenesis, and ECM remodeling. Finally, we observed an enrichment of the AGE-RAGE signaling pathway involved in inflammation, vascular

remodeling, and atherosclerosis. These results suggest that preadipocytes may be involved in the atherogenesis and thus, their adipogenic and ECM-remodeling potential may provide new insights to understand the obesity-related cardiovascular diseases.

Materials and methods

Materials

The recombinant proteins used include: Angiotensin II (Agt II; Novus Biologicales, Cat: NBP1-99199), Interleukin-1β (IL-1β; Sino Biological, Cat: 10139-HNAE), Osteopontin (Spp1; R&D Systems, Cat: 1433-OP), and Transforming growth factor β1 (TGF-β1; Sino Biological, Cat: 10804-HNAC). The siRNAs used were Serpin Family E Member 1 (SERPINE1; Ambion, Lot: ASO2FTIP, ASO2FTIQ), Glyceraldehyde-3-Phosphate Dehydrogenase (GAPDH; Invitrogen, Cat: 4390849), and control siRNA (Ambion, Cat: 4390843).

Cell culture

Human SGBS preadipocytes (Wabitsch et al, 2001), were cultured in T175 flasks in Dulbecco's Modified Eagle Medium (DMEM)/F12 Nut mix (Lonza) containing 33 µM biotin (Sigma), 17 µM pantothenic acid (Sigma), 100 µg/ml of Penicillin/Streptomycin (P/S; Lonza), and 10 % Fetal bovine serum (FBS; Lonza) at 37 °C in 5 % CO_2. The growth medium was changed every 3rd day until the cells reached approx. 80 % confluency.

Adipogenic differentiation

SGBS preadipocytes were differentiated into mature adipocytes to assess the typical gene expression pattern of both SGBS preadipocytes and SGBS adipocytes. Briefly, near confluent SGBS preadipocytes were given adipogenic differentiation for 14 days using QuickDiff medium containing DMEM/F12 Nut mix medium supplemented with 33 µM biotin, 17 µM pantothenic acid, 100 µg/ml P/S, 0.01 mg/ml human transferrin (Sigma), 20 nM human insulin (Sigma), 0.1 µM hydrocortisone (Sigma), 0.2 nM triiodothyronine (Sigma), 25 nM dexamethasone (Sigma), 0.5 µM 3-isobutyl-1-methylxanthine (Sigma), and 2 µM rosiglitazone (Cayman Chemical). The differentiation medium was changed every 3rd day.

Optimization of treatment conditions

Ligand stimulations

SGBS preadipocytes were seeded in 6-well plates at a density of approximately $1.8x10^5$ cells/well and cultured in growth medium until they reached 70-80 % confluency. Before treatments, SGBS preadipocytes were washed with Phosphate buffered saline (PBS) and serum starved in OF medium (DMEM/F12 Nut mix, 33 µM biotin, 17 µM pantothenic acid, 100 µg/ml P/S) for 24 hours. Cells were treated with TGF-β1, IL-1β, Spp1 or Agt II (Table 1) dissolved in OF medium at 37 °C, 5 % CO_2. The ligands used were chosen based on their regulatory potential on the target genes predicted using NicheNet analysis (Browaeys et al, 2020), and the concentrations were selected based on previous publications by choosing a range from lowest to highest concentration (n=2).

Table 1. Recombinant proteins, concentrations, and time points used in the preliminary experiments to optimize the treatment conditions. The concentrations were selected based on previous publications by choosing a range from lowest to highest concentration. As results from the 6-h time point were inconsistent when exposed to TGF-β1 and IL-1β, only 24-h time point was used for Spp1 and Agt II.

Treatment	**Concentrations used in preliminary treatments**	**Duration**
TGF-β1	1 ng/ml, 5 ng/ml, 10 ng/ml	6 h, 24 h
IL-1β	0.5 ng/ml, 1 ng/ml, 5 ng/ml, 10 ng/ml, 15 ng/ml, 20 ng/ml	6 h, 24 h
Spp1	1 µg/ml, 5 µg/ml, 10 µg/ml	24 h
Agt II	0.5 µM, 1 µM, 5 µM	24 h

siRNA transfections

SGBS preadipocytes were seeded in 6-well plates at a density of approximately $1x10^5$ cells/well and cultured in growth medium until they reached approximately 50 % confluency. RNAimax lipofectamine and siRNAs were diluted separately in Opti-MEM containing 10 % FBS, 33 µM of biotin, and 17 µM of pantothenic acid. Transfection mixes were prepared by mixing the RNAimax lipofectamine containing Opti-MEM and the siRNA containing Opti-MEM in ratio 1:1 as follows: for 10 nM concentration, 0.4 µl siRNA was diluted in 200 µl Opti-MEM and mixed with a double volume (0.8 µl) of RNAimax lipofectamine diluted in the same volume (200 µl) of Opti-MEM and incubated for 20 mins at room temperature. Concentrations of 10 nM, 30 nM, and 60 nM were tested. Prior adding the RNAi mix, cells were washed once with PBS and the medium was changed to growth medium without P/S. Cells were then transfected with SERPINE1 I, SERPINE1 II, GAPDH or

control siRNA and incubated for 24 h (37 °C, 5 % CO_2), followed by a PBS wash and 24-h serum starvation as described previously (n=2).

RNA isolation

Total RNA of SGBS preadipocytes was isolated using RNeasy Mini Kit according to the manufacturer's instructions (Qiagen). For better RNA yield, additional washing steps in the protocol were included. The RNA was eluted in 30 µl of RNase-free water and incubated 1 min before the final centrifugation. RNA concentrations, A260/A280, and A60/A230 ratios were quantified with NanoDrop ND-1000 spectrophotometer.

cDNA synthesis

To generate cDNA, 0.2 µg/µl of 20X Random Hexamer Primer (ThermoFisher Scientific) was added to 10 µl of 100 ng/µl RNA, incubated at 65 °C for 5 min, and chilled on ice for 1 min. cDNA mix in total volume of 9 µl containing 1.5 µl H_2O, 4 µl 5X Reaction buffer (250 mM Tris-HCl (pH 8.3 at 25 °C), 250 mM KCl, 20 mM $MgCl_2$, 50 mM DTT; ThermoFisher Scientific), 20 U of RiboLock RNase inhibitor (ThermoFisher Scientific, Cat: EO0382), 1 mM dNTP mix ThermoFisher Scientific, Cat: R0194), and 200 U of Revert Aid Reverse Transcriptase (ThermoFisher Scientific, Cat: EP0442) was then added to each sample and incubated for 10 min at 25 °C, 60 min at 42 °C, and 10 min at 70 °C. Lastly, 5 U of RNaseH (ThermoFisher Scientific, Cat: AM2293) was added to each sample and incubated at 37 °C for 20 minutes.

Real-Time qPCR

Real-time quantitative PCR (RT-qPCR) with SYBR Green chemistry (Roche) using StepOnePlus analyzer (Applied Biosystems) was used for the determination of mRNA expression levels of the selected genes (Table 2). Amplifications were carried out in 17 µl reaction solutions, containing 1x FastStart SYBR Green master mix (Roche), 10 ng/µl cDNA, 10 µM of each specific primer, and 6 µl water. PCR conditions were as follows: 95 °C for 10 min, followed by 40 cycles of 95 °C for 15 s, 60 °C for 15 s, and 72 °C for 30 s; 95 °C for 15 s, 60 °C for 1 min, and 95 °C for 15 s. Each assay was performed with technical triplicates for each of the biological samples. Relative gene expression level for each target gene was calculated with the ΔΔCT method (Livak & Schmittgen, 2001) and normalized to the expression of GAPDH housekeeping gene.

Table 2. Primer sequences of target genes used in the RT-qPCR. The target genes used were selected based on our preliminary results of differentially expressed genes during the atherosclerosis progression *in vivo*. All primers were purchased from Sigma-Aldrich.

Gene	Sequence	Direction
COL1A2	5'-GTGGTTACTACTGGATTGAC	forward
	5'-CTGCCAGCATTGATAGTTTC	reverse
FBN1	5'-AAAGATCTTGATGAGTGTGC	forward
	5'-GTATGGTGTTGGGTAAATCC	reverse
FN1	5'-CCATAGCTGAGAAGTGTTTTG	forward
	5'-CAAGTACAATCTACCATCATCC	reverse
MEG3	5'-ACCCAAGTCTTCTTCCTG	forward
	5'-CTGTGGAGGGATTTCGAG	reverse
SERPINE1	5'-ATCCACAGCTGTCATAGTC	forward
	5'-CACTTGGCCCATGAAAAG	reverse
GAPDH	5'-TCGGAGTCAACGGATTTG	forward
	5'-CAACAATATCCACTTTACCAGAG	reverse

Experimental setup for RNA sequencing

Based on the preliminary results, the concentration giving the maximum response in each ligand treatment was selected to use in the final experiments to RNA-seq. Similarly, the siRNA concentrations showing the maximum knockdown efficiency were chosen. SGBS preadipocytes were seeded in 6 cm dishes and cultured as described previously. Cells were then exposed to either 5 ng/ml of TGF-β1, 10 ng/ml of IL-1β, 10 µg/ml of Spp1, or 0.5 µM of Agt II for 24 hours (37 °C, 5 % CO_2) in OF medium (n=4). siRNA transfections were conducted as described previously with the concentrations of 30 nM SERPINE1 I and 60 nM SERPINE1 II (Table 3). The RNAi mixes were prepared as follows: for 30 nM transfection mix, 3 µl of siRNA was diluted in 250 µl of Opti-MEM and mixed with 6 µl of RNAimax lipofectamine diluted in 250 µl of Opti-MEM. For 60 nM concentration, a double volume (12 µl) of siRNA and RNAimax lipofectamine was used (n=4).

RNeasy Plus Micro Kit (Qiagen) was used to extract the total RNA of SGBS preadipocytes and adipocytes to achieve better RNA yield and purity. Cell lysates were homogenized with QIAshredder spin column by centrifuging for 2 min at full speed. RNA extraction was done according to the manufacturer's instructions, in addition to which two washes with 80 % ethanol were included. Finally, RNA was eluted in 18 µl of RNase-free water, after which the RNA concentration, A260/A280, and A60/A230 ratios were quantified using NanoDrop spectrophotometer (DeNovix DS-11 FX) to check the yield and purity.

Table 3. siRNA target sequences used to silence SERPINE1 expression.

siRNA	**Sequence (5'-3')**
SERPINE1 I	CCAACAUUCUGAGUGCCCATT
SERPINE1 II	AAGCAGCUAUGGGAUUCAATT

Library preparation and RNA sequencing

RNA-seq libraries were prepared using Lexogen QuantSeq 3' mRNA-Seq Library Prep Kit according to the manufacturer's instructions. The optimal cycle number for endpoint PCR was determined using the following PCR program: 98 ℃ 30 s, followed by 35 cycles of 98 ℃ 10 s, 65 ℃ 20 s, and 72 ℃ 30 s; 72 ℃ 1 min, and finally cooled down to 10 ℃. Subsequently, the library amplification was performed using the same PCR conditions for 17 cycles. To ensure the quality, high-sensitivity DNA concentrations of prepared libraries were measured using Qubit 2.0 Fluorometer (Life Technologies), after which the size distribution and successful library preparation of pooled libraries were quantified using Agilent 2100 Bioanalyzer according to the manufacturer's instructions. The sequencing was ran using Illumina NextSeq 500/550.

Data analysis

RNA-seq gene expression quantifications were carried out with R packages under R version 3.5.3. Briefly, cutadapt version 2.8 (Martin, 2011) was used to trim the reads for poly(A), Illumina adapter, and low-quality bases. Following the nf-core RNA-seq pipeline version 1.4.2 (Ewels et al, 2020), reads were aligned to the GRCh37/hg19 human genome with the STAR aligner and counted in transcripts according to Ensembl GRCh37 release 87 gene annotations. The gene biotypes "protein coding", "lincRNA", and "antisense" were retained in the gene expression matrix. To exclude genes with low expression, the filterByExpr function of the EdgeR package version 3.24.3 (Robinson et al, 2010; minimum count: 5; minimum total count: 15) was used. Differential gene expression analysis between treatments was carried out with DESeq2 package version 1.22.2 (Love et al, 2014) using default parameters. Finally, the differentially expressed genes (DEGs) with adjusted p-value (padj) <0.05 and log2fold change (FC) >1.0 or < -1.0 were included in the functional enrichment analysis using g:Profiler. In the functional enrichment analysis, Kyoto Encyclopedia of Genes and Genomes (KEGG) and Reactome (REAC) pathways were assessed using the default parameters.

Results

Optimization of ligand stimulations and RNAi gene knockdowns

Our preliminary data from *in vivo* atherogenic mouse model showed an increased expression of pro-fibrotic genes of mesenchymal stem cells in adipose tissue when the mice were subjected to high-fat diet for 3 months. NicheNet analysis (Browaeys et al, 2020) of the data predicted 228 ligands to have regulatory potential on the 71 DEGs that could thus be responsible for the activation of the fibrotic response (Supplementary Fig. 1). Among the predicted ligands, we selected TGF-β1, IL-1β, Spp1, and Agt II ligands to validate their role in the regulation of target genes in SGBS preadipocytes (Fig. 1). These four ligands were chosen as they showed the highest regulatory potential on the DEGs (Supplementary Fig. 1). First, the ligand concentration and time of stimulation were optimized. Our results showed that the relative gene expression levels measured using RT-qPCR were more consistent at the 24-hour time point compared to 6-hour, as the effect on FC was stronger at the later time point. The highest relative gene expression levels were achieved with the following concentrations: 5 ng of TGF-β1, 10 ng of IL-1β, 10 μg of Spp1, and 0.5 μM of Agt II. At higher concentrations, the FC began to decrease (Supplementary Fig. 2). In RNAi experiments, 30 nM of SERPINE1 I and 60 nM of SERPINE1 II siRNAs showed the highest knockdown efficiency (Supplementary Fig. 3B). These conditions were thus selected for the RNA-seq experiment.

Characterization of common gene expression pattern of mature SGBS adipocytes and SGBS preadipocytes

Differential gene expression analysis between fully differentiated SGBS adipocytes and untreated SGBS preadipocytes was performed to identify basic gene expression profile of both preadipocytes and adipocytes and to see which of the genes are related to adipogenic differentiation. As a result, in total of 2159 genes were upregulated and 2178 genes were downregulated (padj<0.05, log2FC>1.0 or <-1.0, respectively). The functional enrichment analysis of upregulated genes showed the highest enrichment of KEGG pathway "Metabolic pathways" ($p=4.3x10^{-49}$), while the most enriched REAC pathway was "Metabolism" ($p=1.4x10^{-76}$, Supplementary Table 1). The top 15 upregulated genes included mostly lipid and fatty acid metabolism-associated genes such as *GPAM*, *ACLY*, *FASN*, and *ME1*, as well as genes associated with vitamin and cofactor metabolism including *VKORC1L1*, *RETSAT*, and *CYB5A* (Supplementary Table 3). In regard to downregulated genes, i.e., genes expressed predominantly in SGBS preadipocytes, the most enriched KEGG pathway was "Regulation of actin cytoskeleton" ($p=4.48x10^{-14}$), while "Signaling by Rho GTPases" ($p=2.05x10^{-13}$) was the most enriched in REAC (Supplementary Table 2), respectively. The most significant preadipocyte-like genes were associated with extracellular matrix organization or remodeling (*THBS1*, *FGF2*, *TIMP3*), signal transduction (*BDNF*, *SMURF2*), and various heterogeneous functions (Supplementary Table 3).

TGF-β1 induced the expression of genes associated with the extracellular matrix

Next, we studied each ligand stimulation in more detail. In response to TGF-β1, 751 genes were significantly upregulated (padj<0.05, log2FC>1.0) whereas 895 genes were downregulated (padj<0.05, log2FC<-1.0), respectively. The functional enrichment analysis of upregulated genes showed the highest enrichment of KEGG pathway "AGE-RAGE signaling in diabetic complications" ($p=4.65x10^{-7}$) and "Extracellular matrix organization" ($p=2.50x10^{-3}$) in REAC (Supplementary Table 4). The top 15 upregulated genes were mostly associated with extracellular matrix organization (*ADAM19*, *ACTN1*, *SH3PXD2A*, *FBLN5*) and signal transduction (*CDKN2B*, *ACTA2*, *PMEPA1*; Table 4). Regarding the predicted target genes selected for this study, 33 significant genes were differentially expressed in response to TGF- β1, among which 27 genes were upregulated and seven genes were downregulated (padj<0.05, Fig. 1A, Fig. 2). The most enriched pathways related to downregulated genes were "TNF signaling pathway" ($p=5.28x10^{-7}$) in KEGG, and "Cell cycle, mitotic" ($p=2.61x10^{-7}$) in REAC, respectively (Supplementary Table 4). Consequently, the top 15 downregulated genes were mostly associated with immune system (*PTX3*, *SMAD3*, *IFIT3*; Table 4).

Table 4. DEGs and the observed change in log2FC of SGBS preadipocytes exposed to 5 ng/ml of TGF-β1. Results are shown for the 15 most significant genes (padj<0.05, log2FC>1.0 or <-1.0).

GENE	LOG2FC	P.ADJ	GENE	LOG2FC	P.ADJ
CDKN2B	5.35	1.44E-114	**PTX3**	-4.76	7.04E-92
PPME1	3.63	3.41E-113	**KIAA1199**	-4.63	1.50E-67
ADAM19	3.38	1.68E-94	**SMAD3**	-3.48	9.63E-64
ACTA2	4.41	1.60E-93	**USP53**	-4.35	1.16E-62
CTPS1	3.82	6.32E-88	**TGFBR3**	-3.47	2.24E-56
FAM101B	3.00	7.54E-87	**ARL4C**	-2.85	6.77E-45
TSPAN2	5.95	2.98E-74	**IFIT3**	-4.11	5.36E-43
TPM1	3.01	3.08E-71	**CDC42EP4**	-3.90	4.37E-42
ACTN1	2.32	4.18E-70	**CYP1B1**	-2.59	4.40E-42
MRAS	2.04	9.98E-68	**TFPI**	-2.61	1.74E-35
GADD45B	4.14	5.76E-66	**PDE7B**	-4.83	7.48E-33
SH3PXD2A	2.13	1.53E-63	**SLC7A14**	-3.80	4.41E-32
NUAK1	3.80	2.25E-62	**ALDH1A3**	-2.47	2.61E-30
FBLN5	1.94	1.01E-54	**SEMA3A**	-4.14	2.65E-29
GLIPR2	2.57	7.99E-54	**PHLDA1**	-3.82	3.46E-29

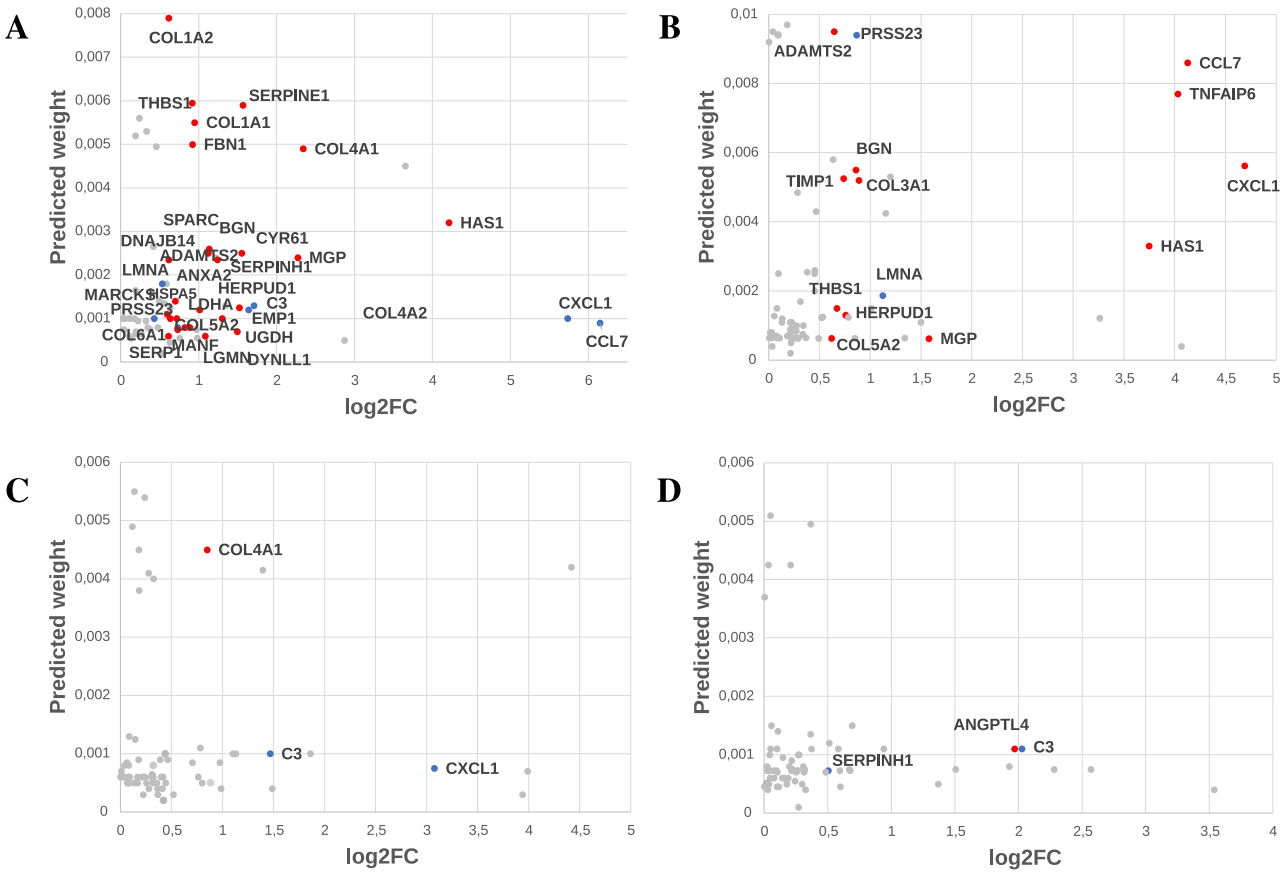

Figure 1. Scatter plots showing the differentially expressed predicted ligand target genes for each ligand. The absolute log2FC is shown in the x-axis, while the predicted weight of each gene is shown in the y-axis. The predicted weight of each gene is based on the NicheNet analysis of DEGs obtained from *in vivo* atherosclerosis progression and the putative ligand interactions. Upregulated genes are shown in red (padj<0.05, log2FC>0), downregulated genes in blue (padj<0.05, log2FC<0), and non-significant genes (padj>0.05) are shown in gray. **A** 33 genes were differentially expressed in response to TGF-β1. A slight positive correlation was detected between the predicted weight and log2FC (Spearman's correlation $r_s = 0.18$). **B** 14 genes were differentially expressed in response to IL-1β; a slight positive correlation was detected (Spearman's correlation $r_s = 0.23$). **C** 3 genes were differentially expressed in response to Agt II, and they showed a strong negative correlation (Spearman's correlation $r_s = -1$). **D** 3 genes were differentially expressed in response to Spp1, and they showed a strong positive correlation (Spearman's correlation $r_s = 0.87$).

IL-1β induced an inflammatory phenotype in SGBS preadipocytes

IL-1β upregulated in total of 380 genes (padj<0.05, log2FC>1.0) and downregulated 253 genes (padj<0.05, log2FC<-1.0), respectively. In terms of upregulated genes, the most enriched pathways were "IL-17 signaling" ($p=6.88 \times 10^{-13}$) in KEGG and "Interleukin-10 signaling" ($p=8.16 \times 10^{-11}$) in REAC (Supplementary Table 5). Consequently, the most significant upregulated genes were related to cytokine signaling (*MMP3*, *HIF1A*, *MMP1*, *PTGS2*, *EGR1*), although *MMP3*, *MMP1*, and *ADAM12* were also associated with extracellular matrix organization (Table 5). In addition, 14 predicted ligand target genes were differentially expressed in response to IL-1β, among which *CCL7*, *TNFAIP6*, *CXCL1*, *BGN*, *TIMP1*, *COL3A1*, *HAS1*, *THBS1*, *HERPUD1*, *ADAMTS2*, *COL5A2*, and *MGP* were upregulated, while *LMNA* and *PRSS23* were downregulated (padj<0.05; Fig. 1B, Fig. 2). The most enriched pathways associated with the downregulated genes were "Steroid biosynthesis"

($p=5.12x10^{-9}$) in KEGG and "Cholesterol biosynthesis" ($p=4.40x10^{-16}$) in REAC (Supplementary Table 5), respectively. Accordingly, the most significant downregulated genes were mostly associated with lipid and cholesterol metabolism or biosynthesis, including *MSMO1*, *LIPA*, *HMGCS1*, *FDFT1*, *LDLR*, and *ACAT2* (Table 5).

Table 5. DEGs and the observed change in log2FC of SGBS preadipocytes exposed to 10 ng/ml of IL-1β. Results are shown for the 15 most significant genes (padj<0.05, log2FC>1.0 or <-1.0).

GENE	LOG2FC	P.ADJ	GENE	LOG2FC	P.ADJ
LRRC15	3.59	8.94E-54	**MSMO1**	-2.14	2.39E-54
AMIGO2	3.28	2.02E-45	**KRT19**	-4.62	5.59E-30
MMP3	3.89	1.32E-43	**IGFBP5**	-2.43	1.46E-29
PAPPA	1.97	1.22E-40	**LIPA**	-2.12	1.11E-27
HIF1A	1.51	2.82E-36	**HMGCS1**	-2.02	1.35E-25
CXCL5	5.20	5.84E-36	**FDFT1**	-1.27	9.41E-23
STEAP2	2.78	2.83E-34	**KRT18**	-2.60	1.07E-22
MMP1	3.87	7.14E-31	**LDLR**	-1.36	3.36E-21
CXCL6	4.96	2.25E-29	**SCUBE3**	-2.29	2.36E-20
CCL5	3.90	5.46E-29	**ACAT2**	-2.12	7.87E-19
ADAM12	1.78	1.04E-27	**ADAMTSL1**	-1.82	9.56E-19
CHAC1	2.47	1.22E-24	**C11ORF87**	-3.57	1.06E-18
PTGS2	4.82	6.03E-22	**GDF5**	-3.88	3.40E-18
NFKBIZ	2.87	2.59E-21	**TRNP1**	-1.46	3.65E-18
EGR1	2.67	1.38E-20	**THSD4**	-1.89	1.06E-17

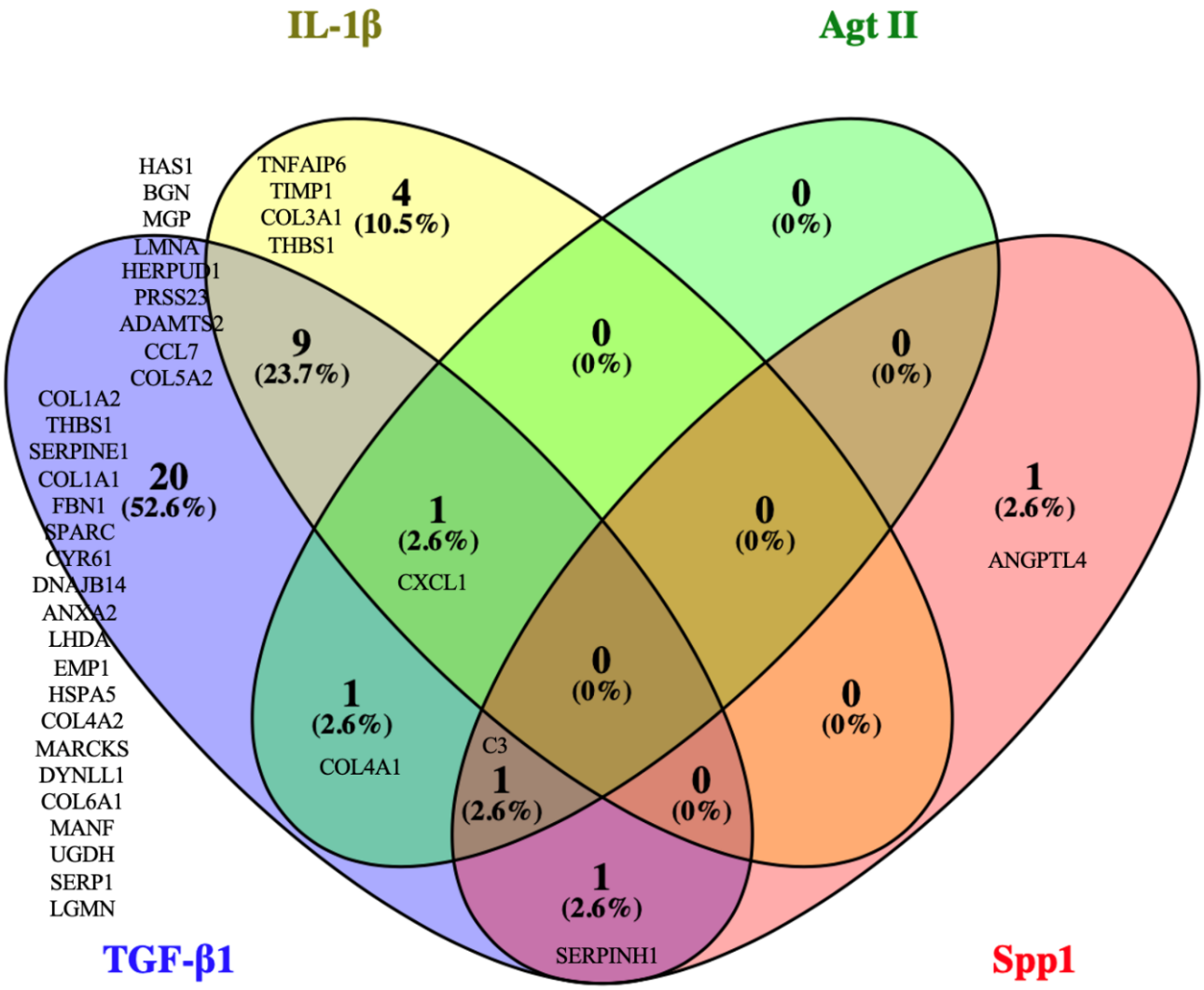

Figure 2. A Venn diagram showing the predicted target genes differentially expressed in response to the ligand treatments. In total of 38 genes were differentially expressed (padj<0.05).

Agt II attenuated cell cycle progression and response to inflammatory factors

In response to Agt II, 106 genes were upregulated (padj<0.05, log2FC>1.0), while 121 genes were downregulated (padj<0.05, log2FC<-1.0), respectively. The most significant upregulated genes were mainly associated with cellular developmental processes (*LBH*, *ACTA2*, *MYH10*, *NEDD9*, *SEMA5A*, *CHAC1*, *SHROOM3*, *DFNA5*; Table 6), and the most enriched KEGG pathway was "Vascular smooth muscle contraction" ($p=6.76x10^{-3}$; Supplementary Table 6). Regarding the predicted ligand target genes, *COL4A1* was upregulated, whereas *C3* and *CXCL1* were downregulated in response to Agt II (padj<0.05, Fig. 1C, Fig. 2). No REAC pathways were associated with the upregulated genes. In turn, the downregulated genes were more heterogeneous including e.g., genes associated with cell cycle (*CDC25B*, *HMGA2*), and response to molecules of bacterial origin (*TNFAIP3*, *PTGFR*, *BDKRB1*, *CXCL1*, *SOD2*; Table 6). The most enriched pathways were "IL-17 signaling pathway" ($p=2.21x10^{-5}$) in KEGG and "Cell cycle, mitotic" ($p=1.98x10^{-2}$) in REAC (Supplementary Table 6).

Table 6. DEGs and the observed change in log2FC of SGBS preadipocytes exposed to 0.5 µM of Agt II. Results are shown for the 15 most significant genes (padj<0.05, log2FC>1.0 or <-1.0).

GENE	LOG2FC	P.ADJ	GENE	LOG2FC	P.ADJ
KCTD20	2.23	6.85E-23	**ALDH1A3**	-1.75	1.90E-14
LBH	1.97	2.37E-17	**TNFAIP3**	-1.84	6.18E-10
ACTA2	1.95	1.19E-16	**PTGFR**	-1.25	2.58E-07
MYH10	1.53	1.67E-12	**C6ORF1**	-1.21	4.82E-07
NEDD9	2.17	5.74E-12	**RGMB**	-1.13	6.75E-07
FAM126A	1.13	2.43E-09	**MT2A**	-1.42	1.35E-06
SEMA5A	1.01	6.63E-09	**BDKRB1**	-2.04	1.56E-06
CHAC1	1.54	1.95E-08	**CDC25B**	-1.17	3.47E-06
SHROOM3	2.27	3.54E-08	**SMYD3**	-1.10	8.75E-06
NID2	1.85	1.32E-07	**RIN1**	-1.45	1.13E-05
FNIP2	1.06	2.58E-07	**THSD4**	-1.13	1.32E-05
CTGF	1.61	2.58E-07	**CXCL1**	-3.07	2.32E-05
TNS1	1.11	3.08E-07	**HMGA2**	-1.46	2.42E-05
C1ORF198	1.46	4.79E-07	**COL13A1**	-1.33	3.81E-05
DFNA5	1.07	4.82E-07	**SOD2**	-1.79	3.91E-05

Spp1 induced the expression of genes related to insulin signaling

In response to Spp1, 91 genes were upregulated (padj<0.05, log2FC>1.0), while 49 genes were downregulated (padj<0.05, log2FC<-1.0), respectively. The most significant upregulated genes were associated with heterogeneous functions, such as signal transduction (*AKAP12*, *PDE4D*), DNA biosynthesis, nucleosome assembly, and cell cycle (*TERC*, *HIST1H4C*, *FBXO4*), or insulin signaling (*PDK4*, *ANGPTL4*, *EPHA5*; Table 7). Additionally, two predicted ligand target genes (*C3*, *SERPINH1*) were downregulated, whereas one gene, *ANGPTL4*, was upregulated (p<0.05, Fig. 1D, Fig. 2). The most enriched KEGG pathway was "TGF-beta signaling pathway" ($p=1.05x10^{-3}$), while no REAC pathways were identified (Supplementary Table 7). In turn, the most significant downregulated genes were mostly related to interleukin signaling (*SOD2*, *TP53*, *ICAM1*, *CCL2*,

VCAM1; Table 7), and the enriched pathways included "Malaria" ($p=1.42x10^{-2}$) in KEGG and "Interleukin-4 and Interleukin-13 signaling" ($p=7.15x10^{-3}$) in REAC (Supplementary Table 7).

Table 7. DEGs and the observed change in log2FC of SGBS preadipocytes exposed to 10 µg/ml of Spp1. Results are shown for the 15 most significant genes (padj<0.05, log2FC>1.0 or <-1.0).

GENE	LOG2FC	P.ADJ	GENE	LOG2FC	P.ADJ
SEMA5A	1.09	1.02E-09	**DRAM1**	-1.66	5.58E-09
FAM43A	1.42	6.46E-08	**GPR174**	-18.92	4.87E-07
AKAP12	1.45	7.82E-07	**SOD2**	-2.05	2.07E-06
PDK4	4.22	2.07E-06	**ARNT2**	-1.88	3.42E-05
WWTR1	1.11	9.93E-06	**WTAP**	-1.01	3.84E-05
AHRR	1.57	1.12E-05	**TP53**	-1.03	6.08E-05
PDE4D	2.86	1.29E-05	**ICAM1**	-2.12	1.07E-04
ANGPTL4	1.97	2.75E-05	**NUPR1**	-1.17	1.37E-04
FBXO5	2.33	2.75E-05	**KIAA1199**	-1.25	2.66E-04
TERC	3.66	4.22E-05	**C3**	-2.03	7.30E-04
HIST1H4C	2.30	5.53E-05	**CPA4**	-1.29	1.18E-03
RP11-485G4.2	1.18	1.37E-04	**FAM101A**	-2.17	1.46E-03
HAS2	1.10	1.66E-04	**SOX13**	-1.61	1.64E-03
EPHA5	1.28	1.66E-04	**CCL2**	-1.74	1.64E-03
BZW1	1.09	1.66E-04	**VCAM1**	-6.26	1.71E-03

SERPINE1 knockdown upregulated genes related to inflammatory response

Finally, we investigated the effects of *SERPINE1* knockdown on downstream gene expression to see if any genes related to coronary artery disease (CAD) were expressed. *SERPINE1* was chosen as it was one of the predicted target genes that has been linked to obesity and CVD (Kaur et al, 2010; Liang et al, 2006). As a result, the knockdown of *SERPINE1* upregulated the expression of 17 genes (padj<0.05, log2FC>1.0), while 59 genes were downregulated (padj<0.05, log2FC<-1.0), respectively. No data regarding KEGG or REAC pathways were provided in g:Profiler. Both up- and downregulated genes were associated with widely heterogeneous functions; the upregulated genes were related to processes such as inflammatory response (*CRORF30*, *PTGER2*), metabolic processes

(*AKR1B10*, *MOCS3*), and transcriptional regulation (*LCOR*, *HOXA9*, *HMGA*; Table 8). In turn, the downregulated genes were associated with, e.g., cell cycle (*CKAP5*, *TXNIP*), cell adhesion (*NRXN3*, *PCDHGA12*), and neurotransmitter transport (*SV2A*, *SLC6A9*; Table 8).

For unknown reason, *SERPINE1* II RNAi did not reduce the *SERPINE1* expression significantly (padj=0.1, log2FC=-0.6).

Table 8. DEGs and the observed change in log2FC of SGBS preadipocytes in response to *SERPINE1* knockdown. Results are shown for the 15 most significant genes (padj<0.05, log2FC>1.0 or <-1.0).

GENE	LOG2FC	P.ADJ	GENE	LOG2FC	P.ADJ
HMGA2	1.72	3.40E-07	**SERPINE1**	-2.61	2.17E-24
HOXA9	1.33	4.24E-06	**CKAP5**	-2.46	6.19E-24
MET	1.53	1.11E-05	**MACF1**	-1.15	1.04E-07
MT2A	1.31	3.39E-05	**NRXN3**	-1.26	1.17E-06
RMND5A	1.50	2.83E-04	**MTRNR2L2**	-6.90	7.16E-06
PPP2R1B	1.04	1.02E-03	**MTDH**	-1.06	1.26E-05
PODXL	1.86	3.77E-03	**SULF1**	-1.09	1.33E-05
ARRDC3	1.01	3.77E-03	**FRMD8**	-1.17	3.83E-05
LCOR	1.13	8.38E-03	**TBC1D13**	-1.29	8.10E-05
AKR1B10	2.17	1.15E-02	**BTBD2**	-1.21	1.69E-04
C5ORF30	1.03	1.85E-02	**AKAP12**	-1.18	2.11E-04
PTGER2	2.06	1.94E-02	**TXNIP**	-1.12	2.82E-04
ZCCHC3	1.10	3.51E-02	**SV2A**	-1.57	1.05E-03
MOCS3	1.09	3.64E-02	**SLC6A9**	-2.17	1.15E-03
POLE2	1.80	4.06E-02	**PCDHGA12**	-3.08	1.15E-03

Discussion

In pro-inflammatory conditions, preadipocytes contribute to the remodeling of the ECM (Keophiphath et al, 2009), a process that happens constantly during obesity and might lead to tissue fibrosis (Halberg et al, 2009). Besides adipose tissue, remodeling of the ECM takes place in the atherosclerotic lesions (Katsuda & Kaji, 2003). Here, we validated the expression of 38 genes, some

of which were associated with the ECM remodeling, in human SGBS preadipocytes that were differentially expressed during the atherosclerosis progression *in vivo*. Moreover, we found that stimulation of SGBS preadipocytes with factors contributing to obesity and atherosclerosis has a wide effect on genes related to adipogenesis, atherosclerosis, and ECM. Together, our findings suggest preadipocytes might be a one potential contributor to the progression of atherosclerosis either directly or indirectly.

One major regulator of remodeling the ECM is TGF-β, as it can reduce the synthesis of ECM-degrading proteases and increase the synthesis of their inhibitors (Roberts et al, 1992). In line with this, TGF-β1 upregulated 14 predicted target genes associated with the ECM, among which *COL4A2*, *COL4A1*, and *SERPINH1* have recently been proposed as a risk genes or loci for CAD (Howson et al, 2017; Zheng et al, 2020). Furthermore, among the predicted target genes, *THBS1*, *SERPINE1*, and *BGN* are highly expressed in atherosclerotic plaques of both mice and human (Moura et al, 2008; Riessen et al, 1994; Schneiderman et al, 1992). In turn, elevated plasma *SPARC* levels have been detected in patients with CAD (Takahashi et al, 2001), whereas *FBN1* is suggested to be a potential biomarker for predicting the severity of acute coronary syndrome with unstable angina pectoris (Acara et al, 2018). Besides their contribution to ECM and atherosclerosis, these genes are upregulated in obesity and contribute to adipogenesis. For example, FBN1 is proposed to mediate changes in the ECM required for lipid deposition, and mutations in *FBN1* gene are associated with depletion of SAT (Davis et al, 2016). THBS1 stimulates preadipocyte proliferation and may thus increase the adiposity via hyperplasia (Kong et al, 2013), whereas BGN may reduce the proliferation of preadipocytes (Ward & Ajuwon, 2011). In addition, both SERPINE1 and SPARC are able to inhibit adipogenic differentiation (Liang et al, 2006, Nie & Sage, 2009). Overall, these results suggest that during obesity, preadipocytes produce ECM-associated factors, such as THBS1, FBN1, BGN, SPARC, and SERPINE1, that may further promote lipid deposition into the adipose and/or other tissues through ECM accumulation and remodeling, and/or affecting the differentiation capacity of preadipocytes and reducing the number of lipid-storing mature adipocytes. Altogether, ectopic lipid deposition promotes obesity-related comorbities and increases the risk of atherosclerosis and CVD (Lim & Meigs, 2014). Moreover, *THBS1*, *FBN1*, *BGN*, *SPARC*, *COL4A2*, *COL4A1*, *SERPINH1*, and *SERPINE1* are associated with atherosclerosis, although it remains unclear what is the role of preadipocytes expressing these factors during the disease progression.

In addition, we observed an enrichment of the AGE-RAGE signaling pathway when SGBS preadipocytes were exposed to TGF-β1, IL-1β, or Agt II. It is noteworthy that the enrichment of AGE-RAGE signaling pathway was already detected in the preliminary data on preadipocytes during

the atherosclerosis progression *in vivo* (unpublished data). In the present study, differentially expressed predicted ligand target genes involved in this pathway contained *COL1A1*, *COL1A2*, *COL3A1*, *COL4A1*, *COL4A2*, and *SERPINE1*. The AGE-RAGE axis has been shown to regulate adipocyte-ECM crosstalk (Strieder-Barboza et al, 2019) and adiposity, and it is also associated with atherosclerosis in non-diabetic conditions (Ueno et al, 2010). Thus, this pathway could be one potential mechanism explaining the involvement of preadipocytes in the development obesity-related complications and atherosclerosis. Another example of genes included in the AGE-RAGE axis is *EGR1*, a transcription factor induced by IL-1β that is a master regulator of CVD related genes (Khachigian, 2006) and contributes to vascular dysfunction in the AGE-RAGE signaling pathway. Therefore, the expression of EGR1 under pro-inflammatory and/or obesogenic conditions can promote adipose tissue dysfunction that may further lead to systemic consequences (Zhang et al, 2013) not only through adipose dysfunction, but also inducing the expression of other genes related to CVD.

Visceral adipose tissue inflammation may be considered as a causative factor for CVD (Ohman et al, 2008), and adipose tissue is able to synthesize cytokines that participate in the atherosclerotic process (Berg & Scherer, 2005). Here, we detected an enrichment of inflammatory pathways when SGBS cells were exposed to IL-1β. In addition to pro-inflammatory chemokines and cytokines, the expression of some of the predicted target genes, such as *BGN*, correlates with adipose tissue inflammation (Adapala et al, 2012). Moreover, *MMP1* and *MMP3* that were associated with IL signaling not only contribute to the remodeling of adipose tissue ECM but are also involved in the atherosclerotic process. MMPs degrade the matrix between vascular intima and media that allows the migration of smooth muscle cell to the intima and promoting the plaque expansion (Vacek et al, 2015). Human preadipocytes have been shown to express *MMP1* and *MMP3* in pro-inflammatory conditions *in vitro* (Gao & Bing, 2011), but whether preadipocytes can contribute to vascular remodeling through MMP activation is unclear. We also found an increased expression of *PAPPA*, another pro-inflammatory factor and an extracellular enzyme, that contributes to the development of atherosclerosis indirectly via regulating the bioavailability of insulin-like growth factor. Conover et al (2013) have shown that visceral preadipocytes are more prone to express *PAPPA* compared to subcutaneous preadipocytes, and they proposed that PAPPA may regulate depot-specific adipogenesis in a paracrine manner similarly as it participates in the progression of atherosclerosis. It would be relevant to investigate if there is any correlation between the *PAPPA* expression of visceral preadipocytes and atherogenesis, as the *PAPPA* expression has been proposed as a candidate marker for the early plaque instability (Bayes-Genis et al, 2001).

Even though both Agt II and Spp1 affected only few of the predicted target genes, we found that Agt II induced the expression of *CTGF* that is an important regulator of fibrinogenesis and positively correlated with adiposity and insulin resistance (Yoshino et al, 2019). Also, endothelin-1 (*EDN1*) that promotes adipocyte lipolysis during obesity (Eriksson et al, 2009) was upregulated, although earlier studies have reported the antilipolytic potential of Agt II (Goossens et al, 2004). Nonetheless, EDN1 is widely known to be involved in the atherogenic process via its vasoconstrictive, mitogenic, and proliferative properties, as well as its interactions with other atherogenic factors, such as cytokines and growth factors (Mathew et al, 1996). Although we found an upregulation of EDN1 in preadipocytes, it is mainly produced by endothelial cells (Thorin & Webb, 2013). As the vascular inflammation plays a pivotal role in atherosclerosis, pro-inflammatory preadipocytes capable to signal endothelial cells could have disease-promoting effects on the vasculature, as reported by Parvizi et al (2021). Thus, even though preadipocytes could not produce EDN1 or other factors contributing to the vascular inflammation themselves, they may affect these processes indirectly via communicating with endothelial cells. In terms of atherosclerosis, we also found an upregulation of *SEMA5A*, a risk locus for CAD (Van der Harst & Verweij, 2018), when preadipocytes were exposed to Agt II or Spp1. As SEMA5A can mediate the ECM degradation through activation of MMP9 in endothelial cells (Sadanandam et al, 2010) it would be of interest to know if it has similar effects on preadipocytes. However, there are no previous publications concerning (pre)adipocytes and SEMA5A and thus, further studies would be needed to clarify its functionality on preadipocytes.

Obesity is associated with both insulin resistance and dyslipidemia that are commonly known risk factors for CVD (Ormazabal et al, 2018). When exposed to Spp1, we observed an upregulation of *ANGPTL4*, one of the predicted target genes, that is involved in both insulin signaling and lipid metabolism. *ANGPTL4* inhibits lipoprotein lipase activity which prevents the uptake of triglycerides into adipose tissue (Cushing et al, 2017). This results in increased plasma triacylglycerol level which is a risk factor for CVD. In turn, ANGPTL4 deficiency in adipose tissue leads to increased lipid uptake by adipocytes that reduces the ectopic lipid accumulation and may prevent the development of atherosclerosis (Aryal et al, 2018). Although upregulation of *ANGPTL4* has earlier been reported at the late stage of adipogenic differentiation (Yin et al, 2014), our data suggest it is also expressed by preadipocytes in obesogenic/atherogenic conditions. Hence, whether *ANGPTL4* expression by preadipocytes under atherogenic conditions affects their ability to accumulate lipids during the differentiation would be an interesting topic to research, especially in the context of obesity and insulin resistance. Furthermore, *SERPINE1*, one of the predicted target genes, is associated with obesity, inflammation, and atherosclerosis (Alessi & Juhan-Vague, 2006). Besides the induction of

SERPINE1 in response to TGF-β1 exposure, we performed *SERPINE1* knockdown to investigate its effects on downstream gene expression. In terms of adipogenesis, our results show controversy as several adipogenesis-associated genes were both up- and downregulated, including *HMGA2*, *LCOR*, *MTDH*, and *TXNIP*. Instead, earlier studies suggest that *SERPINE1* deficiency promotes the development of obesity (Liang et al, 2006). The controversy observed here might be due to original study by Liang et al (2006) being conducted in both differentiating primary (pre)adipocytes from *PAI-1* null mice and mouse 3T3-L1 (pre)adipocytes. Instead of differentiating mouse (pre)adipocytes, we used human SGBS preadipocytes not induced to differentiate and hence, it cannot be concluded what is the biological importance of these genes in human preadipocytes. However, it seems plausible that *SERPINE1* mediates downstream effects on adipogenesis, although whether it promotes or attenuates the preadipocyte differentiation remains controversial.

Although we have shown that *SERPINE1* expression is induced in preadipocytes during the atherosclerosis progression *in vivo* (unpublished data), we did not find major downstream effects of *SERPINE1* knockdown on atherogenesis or CAD. An exception was the upregulation of *HOXA9* which overexpression has been shown to inhibit the expression of adhesion molecules, such as ICAM-1 and VCAM-1 (Trivedi et al, 2007), and *TXNIP,* which upon gene knockout has shown to be protective against atherosclerosis development *in vivo* (Byon et al, 2015). Nonetheless, Chatterjee et al (2013) have shown that perivascular adipocytes highly express SERPINE1 and hence, they suggested that PVAT adipocytes might have potential to modulate vascular inflammation through their ability to signal to both endothelial and inflammatory cells in atherosclerosis (Chatterjee et al, 2013). Therefore, it will require further studies to investigate the potential effects of *SERPINE1* and preadipocytes on atherosclerosis. In addition, it cannot be ignored that *SERPINE1* expression by mature adipocytes may play more important role in the atherosclerosis compared to preadipocytes, as increased *SERPINE1* expression has been characterized during the adipogenic differentiation and in mature adipocytes (Serrano et al, 2009). However, data from human adipose tissue suggest that *SERPINE1* is predominantly expressed by the stromal vascular fraction of the adipose tissue (Bastelica et al, 2002). Additionally, the two *SERPINE1* siRNAs used showed different knockdown efficiency. It is known that siRNAs targeting different regions of a gene can have different knockdown efficiencies (Han, 2018), and the second *SERPINE1* siRNA was less effective already in the optimization stage. Considering the differences between the knockdown efficiency and thus the downstream gene expression of the two *SERPINE1* siRNAs used, a deeper investigation is needed to assess the downstream effects of *SERPINE1* knockdown in SGBS preadipocytes.

Collectively, using an experimental *in vitro* model of human SGBS preadipocytes, we validated the expression of 38 genes out of 71 predicted ligand target genes differentially expressed during the atherosclerosis progression *in vivo*. Furthermore, we showed that exposure of SGBS preadipocytes to obesogenic/atherogenic factors induces changes in their gene expression associated with the ECM, adipogenesis, and atherosclerosis. Some of the DEGs were included in the AGE-RAGE signaling pathway that is proposed to be a one contributor to atherosclerosis. Hence, we propose that preadipocytes might have atherogenesis-promoting effects under obesogenic and/or atherogenic conditions, possibly through the AGE-RAGE signaling pathway and/or via paracrine signaling to vascular cells. Nevertheless, more studies are needed to elucidate the biological importance of the AGE-RAGE signaling in human preadipocytes and the possible interactions of preadipocytes with other cell types in the atherosclerotic environment. In brief, our results suggest that preadipocytes may be involved in the atherogenesis and thus, their adipogenic and ECM-remodeling potential, as well as interaction with other cell types, may provide new insights to understand the obesity-related cardiovascular diseases.

Acknowledgements

I would like to acknowledge the following persons: Uma Thanigai Arasu, thank you for the supervision, planning, and help with the practical work. Minna Kaikkonen-Määttä, thank you for the supervision and possibility to execute this thesis. Tuula Salonen, thank you for technical help. Tiit Örd, thank you for handling the RNA-seq data. Finally, I would like to thank the whole CADGEN group for the inspiring and supporting environment to execute my thesis.

Supplementary material

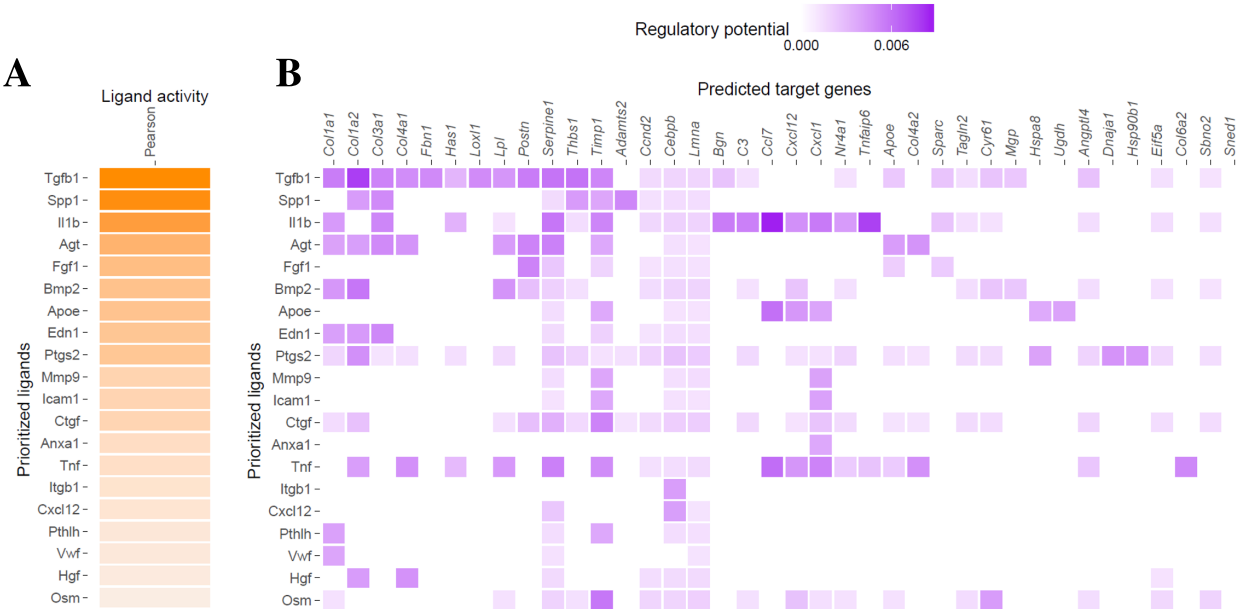

Supplementary Figure 1. NicheNet analysis showing prioritized ligands based on their potential to regulate DEGs observed in mesenchymal stem cells of LDLR$^{-/-}$/ApoB$^{100/100}$ mice subjected to high-fat diet for 3 months. **A** Ligand activity prediction on the DEGs. Results are shown for the 20 (of 228) ligands best predicting the DEGs. Pearson correlation coefficient indicating the ability of each ligand to regulate the differentially expressed target genes are shown. **B** Ligand-target interactions denoting the regulatory potential between ligands and the target genes. In total of 79 genes were upregulated in mesenchymal stem cells, among which 71 genes were present as targets in the overall ligand-target matrix. Results are shown for the 38 (of 71) predicted target genes. The NicheNet analysis and image generation courtesy of Dr. Tiit Örd.

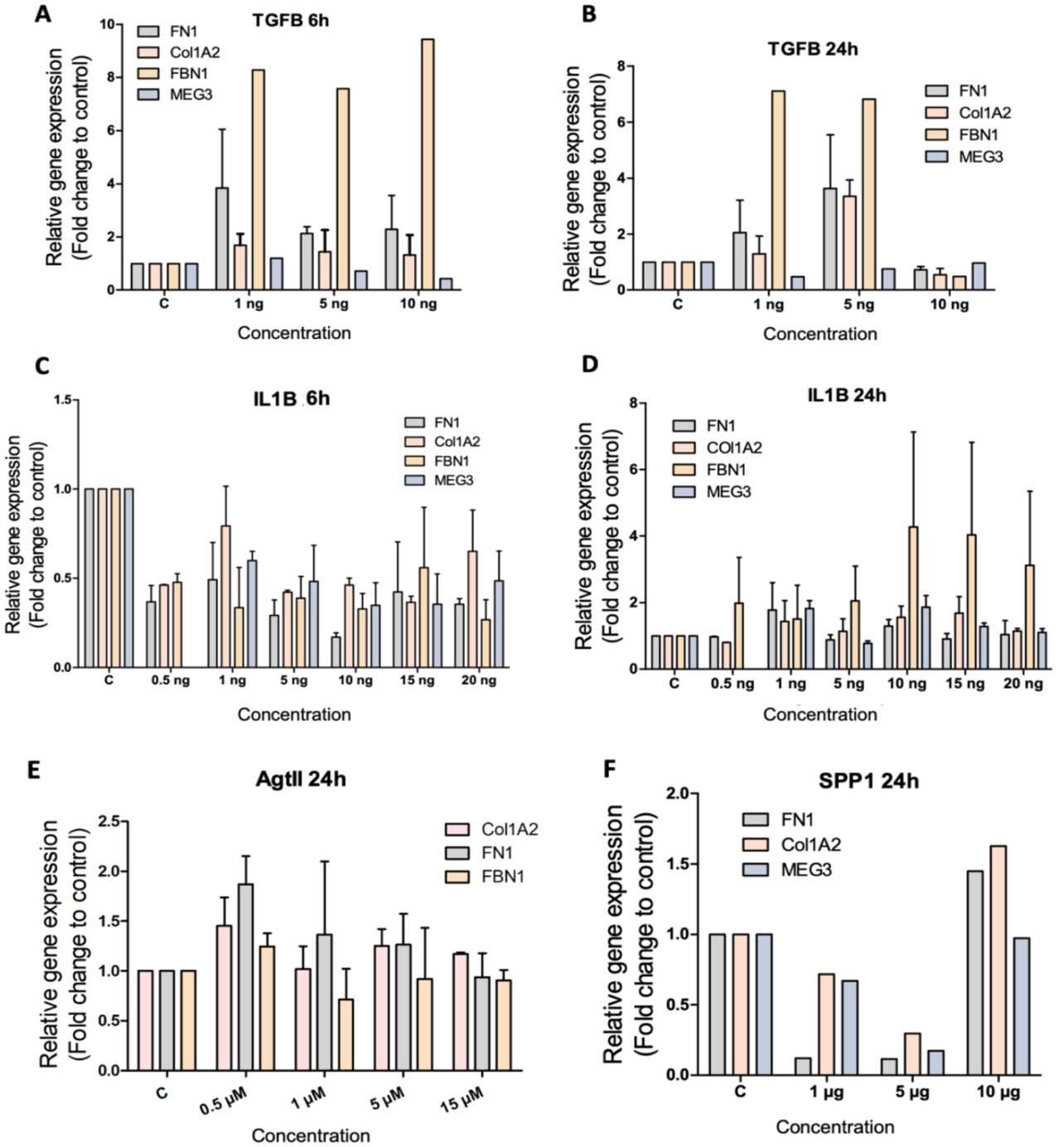

Supplementary Figure 2. Relative gene expression of *COL1A2*, *FBN1*, *FN1*, and *MEG3* of SGBS preadipocytes treated with **A-B** TGF-β1, **C-D** IL-1β, **E** Agt II, and **F** Spp1. The concentrations used were selected based on previous publications by choosing a concentration range from lowest to highest. For Spp1 and Agt II, only 24-hour time point was tested. The following concentrations from 24 h treatments were selected for further experiments: TGF-β1 5 ng, IL-1β 10 ng, Agt II 0.5 µM, Spp1 10 µg. The relative gene expression levels of technical triplicates for each of the biological samples were measured using RT-qPCR and the ΔΔCT method. n=2, mean+SEM.

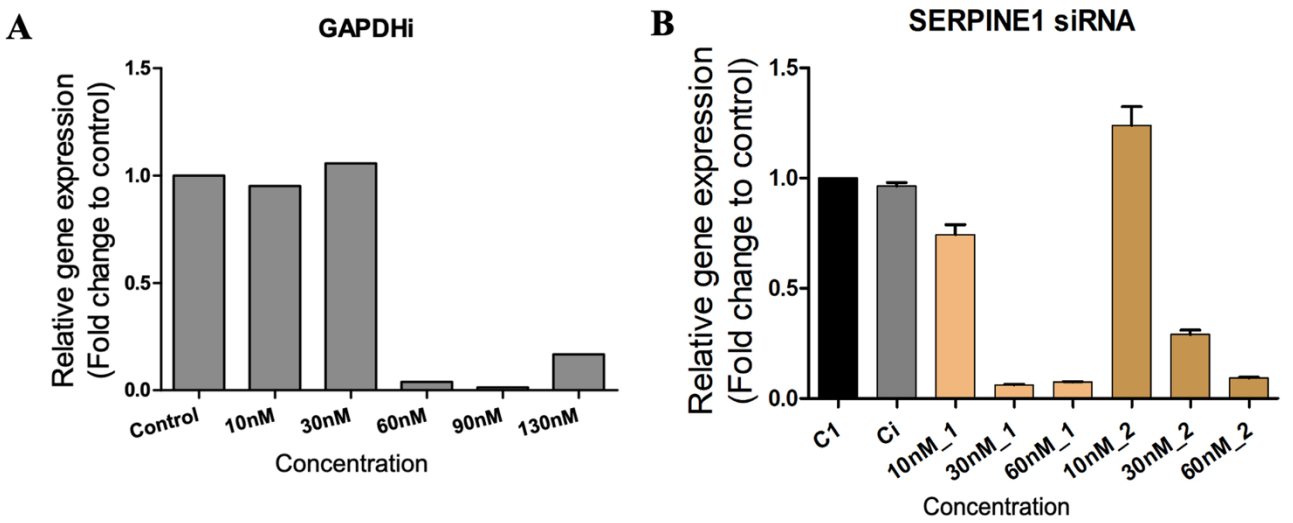

Supplementary Figure 3. Relative gene expression of **A** *GAPDH* and **B** *SERPINE1* of SGBS preadipocytes treated with the respective RNAi. Two different siRNAs were tested for *SERPINE1,* of which concentrations of 30 nM and 60 nM showed the most efficient knockdown of *SERPINE1*. n=2, mean+SEM.

Supplementary Table 1. Enriched KEGG and REAC pathways related to DEGs that were upregulated (padj<0.05, log2FC>1.0) between fully differentiated SGBS adipocytes and untreated SGBS preadipocytes. Results are shown for the 15 most enriched pathways. The functional enrichment analysis was performed using g:Profiler with default parameters.

GO.ID	DESCRIPTION	P.VAL	GO.ID	DESCRIPTION	P.VAL
KEGG:01100	Metabolic pathways	4.34E-49	**REAC:R-HSA-1430728**	Metabolism	1.45E-76
KEGG:00280	Valine, leucine and isoleucine degradation	3.04E-24	**REAC:R-HSA-1428517**	The citric acid (TCA) cycle and respiratory electron transport	1.47E-35
KEGG:01200	Carbon metabolism	2.35E-15	**REAC:R-HSA-611105**	Respiratory electron transport	3.30E-26
KEGG:01212	Fatty acid metabolism	1.86E-14	**REAC:R-HSA-556833**	Metabolism of lipids	7.25E-26
KEGG:00640	Propanoate metabolism	6.47E-14	**REAC:R-HSA-163200**	Respiratory electron transport, ATP synthesis by chemiosmotic coupling, and heat production by uncoupling proteins	1.26E-23
KEGG:00071	Fatty acid degradation	8.80E-14	**REAC:R-HSA-8978868**	Fatty acid metabolism	4.19E-16
KEGG:04714	Thermogenesis	1.51E-13	**REAC:R-HSA-71406**	Pyruvate metabolism and Citric Acid (TCA) cycle	3.17E-13
KEGG:04932	Non-alcoholic fatty liver disease	1.93E-12	**REAC:R-HSA-196854**	Metabolism of vitamins and cofactors	1.95E-12
KEGG:00020	Citrate cycle (TCA cycle)	5.97E-12	**REAC:R-HSA-191273**	Cholesterol biosynthesis	1.15E-10
KEGG:00620	Pyruvate metabolism	7.12E-12	**REAC:R-HSA-6799198**	Complex I biogenesis	4.93E-10
KEGG:03320	PPAR signaling pathway	9.36E-12	**REAC:R-HSA-70895**	Branched-chain amino acid catabolism	1.73E-09
KEGG:00190	Oxidative phosphorylation	7.27E-11	**REAC:R-HSA-77289**	Mitochondrial Fatty Acid Beta-Oxidation	4.46E-09
KEGG:04146	Peroxisome	6.88E-09	**REAC:R-HSA-8957322**	Metabolism of steroids	2.60E-07

KEGG:05012	Parkinson disease	7.39E-08	**REAC:R-HSA-2426168**	Activation of gene expression by SREBF (SREBP)	2.98E-07
KEGG:05020	Prion disease	2.06E-07	**REAC:R-HSA-71403**	Citric acid cycle (TCA cycle)	1.78E-06

Supplementary Table 2. Enriched KEGG and REAC pathways related to DEGs that were downregulated (padj<0.05, log2FC<-1.0) between fully differentiated SGBS adipocytes and untreated SGBS preadipocytes. Results are shown for the 15 most enriched pathways. The functional enrichment analysis was performed using g:Profiler with default parameters.

GO.ID	DESCRIPTION	P.VAL	GO.ID	DESCRIPTION	P.VAL
KEGG:04810	Regulation of actin cytoskeleton	4.21E-14	**REAC:R-HSA-194315**	Signaling by Rho GTPases	1.95E-13
KEGG:05205	Proteoglycans in cancer	1.10E-09	**REAC:R-HSA-69278**	Cell Cycle, Mitotic	9.57E-11
KEGG:04510	Focal adhesion	4.27E-09	**REAC:R-HSA-195258**	RHO GTPase Effectors	1.39E-10
KEGG:05200	Pathways in cancer	1.03E-08	**REAC:R-HSA-1640170**	Cell Cycle	3.83E-09
KEGG:05135	Yersinia infection	2.72E-08	**REAC:R-HSA-5663220**	RHO GTPases Activate Formins	5.86E-09
KEGG:04015	Rap1 signaling pathway	3.18E-08	**REAC:R-HSA-109582**	Hemostasis	3.49E-08
KEGG:04668	TNF signaling pathway	4.82E-08	**REAC:R-HSA-2500257**	Resolution of Sister Chromatid Cohesion	3.72E-08
KEGG:04390	Hippo signaling pathway	2.78E-07	**REAC:R-HSA-9648025**	EML4 and NUDC in mitotic spindle formation	6.00E-08
KEGG:04933	AGE-RAGE signaling pathway in diabetic complications	5.21E-07	**REAC:R-HSA-68877**	Mitotic Prometaphase	2.75E-07
KEGG:04010	MAPK signaling pathway	2.77E-06	**REAC:R-HSA-141444**	Amplification of signal from unattached kinetochores via a MAD2 inhibitory signal	3.06E-07
KEGG:05130	Pathogenic Escherichia coli infection	5.14E-06	**REAC:R-HSA-141424**	Amplification of signal from the kinetochores	3.06E-07
KEGG:05163	Human cytomegalovirus infection	7.15E-06	**REAC:R-HSA-69618**	Mitotic Spindle Checkpoint	2.12E-06
KEGG:04218	Cellular senescence	7.62E-06	**REAC:R-HSA-69620**	Cell Cycle Checkpoints	1.81E-05
KEGG:04014	Ras signaling pathway	9.18E-06	**REAC:R-HSA-1280215**	Cytokine Signaling in Immune system	3.56E-05
KEGG:04151	PI3K-Akt signaling pathway	1.22E-05	**REAC:R-HSA-1474244**	Extracellular matrix organization	6.66E-05

Supplementary Table 3. DEGs and the observed change in log2FC between fully differentiated SGBS adipocytes and SGBS preadipocytes. Results are shown for the 15 most significant genes (padj<0.05, log2FC>1.0 or <-1.0).

GENE	LOG2FC	P.ADJ	GENE	LOG2FC	P.ADJ
STOM	4.79	2.96E-257	CKAP4	-2.18	1.33E-87
GPAM	6.54	1.84E-228	TIMP3	-3.6	4.83E-84
ACLY	3.99	3.10E-228	RAB3B	-2.97	4.02E-81
PRDX6	2.94	5.41E-210	ALCAM	-2.78	1.41E-76
ECHDC1	4.20	4.73E-207	THBS1	-2.57	1.58E-76
VKORC1L1	3.81	1.01E-206	MYADM	-3.38	1.02E-73
RETSAT	4.53	3.65E-203	BDNF	-3.40	1.69E-71
MKNK2	4.47	1.35E-192	SMURF2	-3.02	3.18E-68
CYB5A	5.31	4.99E-171	PRRX1	-2.38	9.98E-67
FASN	5.74	9.09E-168	TPM1	-2.88	1.47E-65
ME1	4.36	1.35E-166	FGF2	-3.35	7.70E-65
MME	5.50	4.65E-143	RAI14	-2.35	1.00E-64
SERPINF1	5.31	1.01E-136	BEX1	-2.89	1.56E-63
ACSS2	6.71	1.17E-133	EMP1	-3.16	4.40E-63
IDH1	4.23	1.38E-130	PPP1R18	-2.7	7.27E-63

Supplementary Table 4. Enriched KEGG and REAC pathways related to DEGs in SGBS preadipocytes exposed to TGF-β1. Results are shown for the 10 most enriched pathways. Pathways related to upregulated genes (padj<0.05, log2FC>1.0) are shown on the left, and pathways related to downregulated genes (padj<0.05, log2FC<-1.0) are shown on the right. The functional enrichment analysis was performed using g:Profiler with default parameters.

GO.ID	DESCRIPTION	P.VAL	GO.ID	DESCRIPTION	P.VAL
KEGG:04933	AGE-RAGE signaling pathway in diabetic complications	4.65E-07	**KEGG:04668**	TNF signaling pathway	5.28E-07
KEGG:04350	TGF-beta signaling pathway	5.65E-06	**KEGG:04110**	Cell cycle	3.35E-04
KEGG:04015	Rap1 signaling pathway	3.20E-05	**KEGG:04621**	NOD-like receptor signaling pathway	7.57E-04
KEGG:05200	Pathways in cancer	4.68E-05	**KEGG:04064**	NF-kappa B signaling pathway	1.50E-03
KEGG:04550	Signaling pathways regulating pluripotency of stem cells	1.69E-04	**KEGG:04657**	IL-17 signaling pathway	2.26E-03

KEGG:04390	Hippo signaling pathway	1.75E-04	**KEGG:05200**	Pathways in cancer	3.40E-03
KEGG:04510	Focal adhesion	1.78E-04	**KEGG:04061**	Viral protein interaction with cytokine and cytokine receptor	3.76E-03
KEGG:05205	Proteoglycans in cancer	2.74E-04	**KEGG:04010**	MAPK signaling pathway	7.78E-03
KEGG:04810	Regulation of actin cytoskeleton	7.21E-04	**KEGG:05418**	Fluid shear stress and atherosclerosis	1.75E-02
KEGG:05230	Central carbon metabolism in cancer	1.07E-03	**KEGG:05323**	Rheumatoid arthritis	2.04E-02
REAC:R-HSA-1474244	Extracellular matrix organization	2.50E-03	**REAC:R-HSA-69278**	Cell Cycle, Mitotic	2.61E-07
REAC:R-HSA-446353	Cell-extracellular matrix interactions	4.21E-03	**REAC:R-HSA-2500257**	Resolution of Sister Chromatid Cohesion	8.57E-07
REAC:R-HSA-9006936	Signaling by TGFB family members	1.14E-02	**REAC:R-HSA-68877**	Mitotic Prometaphase	1.27E-06
REAC:R-HSA-9006934	Signaling by Receptor Tyrosine Kinases	1.33E-02	**REAC:R-HSA-1640170**	Cell Cycle	9.94E-06
REAC:R-HSA-170834	Signaling by TGF-beta Receptor Complex	1.40E-02	**REAC:R-HSA-141444**	Amplification of signal from unattached kinetochores via a MAD2 inhibitory signal	1.65E-05
REAC:R-HSA-445355	Smooth Muscle Contraction	1.65E-02	**REAC:R-HSA-141424**	Amplification of signal from the kinetochores	1.65E-05
REAC:R-HSA-9031628	NGF-stimulated transcription	1.89E-02	**REAC:R-HSA-69618**	Mitotic Spindle Checkpoint	4.93E-05
REAC:R-HSA-162582	Signal Transduction	2.34E-02	**REAC:R-HSA-69620**	Cell Cycle Checkpoints	5.26E-05
REAC:R-HSA-3000178	ECM proteoglycans	3.38E-02	**REAC:R-HSA-1280215**	Cytokine Signaling in Immune system	7.29E-05
REAC:R-HSA-2173793	Transcriptional activity of SMAD2/SMAD3:SMAD4 heterotrimer	3.50E-02	**REAC:R-HSA-68882**	Mitotic Anaphase	1.04E-04

Supplementary Table 5. Enriched KEGG and REAC pathways related to DEGs in SGBS preadipocytes exposed to IL-1β. Results are shown for the 10 most enriched pathways. Pathways related to upregulated genes (padj<0.05, log2FC>1.0) are shown on the left, and pathways related to downregulated genes (padj<0.05, log2FC<-1.0) are shown on the right. The functional enrichment analysis was performed using g:Profiler with default parameters.

GO.ID	DESCRIPTION	P.VAL	GO.ID	DESCRIPTION	P.VAL
KEGG:04657	IL-17 signaling pathway	6.88E-13	**KEGG:00100**	Steroid biosynthesis	5.12E-09
KEGG:04668	TNF signaling pathway	2.37E-11	**KEGG:00900**	Terpenoid backbone biosynthesis	5.65E-07
KEGG:05323	Rheumatoid arthritis	5.17E-10	**KEGG:01100**	Metabolic pathways	1.46E-03
KEGG:04060	Cytokine-cytokine receptor interaction	8.31E-06	**REAC:R-HSA-191273**	Cholesterol biosynthesis	4.40E-16

KEGG:04061	Viral protein interaction with cytokine and cytokine receptor	1.73E-05	**REAC:R-HSA-2426168**	Activation of gene expression by SREBF (SREBP)	6.15E-11
KEGG:04933	AGE-RAGE signaling pathway in diabetic complications	2.20E-05	**REAC:R-HSA-8957322**	Metabolism of steroids	7.70E-11
KEGG:04064	NF-kappa B signaling pathway	1.22E-03	**REAC:R-HSA-1655829**	Regulation of cholesterol biosynthesis by SREBP (SREBF)	1.04E-10
KEGG:05167	Kaposi sarcoma-associated herpesvirus infection	1.89E-03	**REAC:R-HSA-6807062**	Cholesterol biosynthesis via lathosterol	1.45E-05
KEGG:05134	Legionellosis	2.83E-03	**REAC:R-HSA-6807047**	Cholesterol biosynthesis via desmosterol	1.45E-05
KEGG:04978	Mineral absorption	3.66E-03	**REAC:R-HSA-556833**	Metabolism of lipids	1.16E-04
REAC:R-HSA-6783783	Interleukin-10 signaling	8.16E-11			
REAC:R-HSA-449147	Signaling by Interleukins	1.73E-10			
REAC:R-HSA-6785807	Interleukin-4 and Interleukin-13 signaling	4.55E-09			
REAC:R-HSA-1280215	Cytokine Signaling in Immune system	4.39E-08			
REAC:R-HSA-380108	Chemokine receptors bind chemokines	6.88E-07			
REAC:R-HSA-5661231	Metallothioneins bind metals	1.43E-05			
REAC:R-HSA-375276	Peptide ligand-binding receptors	5.50E-05			
REAC:R-HSA-5660526	Response to metal ions	8.82E-05			
REAC:R-HSA-373076	Class A/1 (Rhodopsin-like receptors)	5.83E-04			
REAC:R-HSA-9031628	NGF-stimulated transcription	5.98E-03			

Supplementary Table 6. Enriched KEGG and REAC pathways related to DEGs in SGBS preadipocytes exposed to Agt II. Pathways related to upregulated genes (padj<0.05, log2FC>1.0) are shown on the left, and pathways related to downregulated genes (padj<0.05, log2FC<-1.0) are shown on the right. The functional enrichment analysis was performed using g:Profiler with default parameters.

GO.ID	DESCRIPTION	P.VAL	GO.ID	DESCRIPTION	P.VAL
KEGG:04270	Vascular smooth muscle contraction	6.76E-03	**KEGG:04657**	IL-17 signaling pathway	2.21E-05
KEGG:04933	AGE-RAGE signaling pathway in diabetic complications	1.70E-02	**KEGG:04668**	TNF signaling pathway	1.03E-03
			KEGG:04610	Complement and coagulation cascades	2.59E-02
			KEGG:05323	Rheumatoid arthritis	3.21E-02

			KEGG:04750	Inflammatory mediator regulation of TRP channels	5.00E-02
			REAC:R-HSA-69278	Cell Cycle, Mitotic	1.98E-02
			REAC:R-HSA-373076	Class A/1 (Rhodopsin-like receptors)	3.52E-02

Supplementary Table 7. Enriched KEGG and REAC pathways related to DEGs in SGBS preadipocytes exposed to Spp1. Pathways related to upregulated genes (padj<0.05, log2FC>1.0) are shown on the left, and pathways related to downregulated genes (padj<0.05, log2FC<-1.0) are shown on the right. The functional enrichment analysis was performed using g:Profiler with default parameters.

GO.ID	DESCRIPTION	P.VAL	GO.ID	DESCRIPTION	P.VAL
KEGG:04350	TGF-beta signaling pathway	1.05E-03	**KEGG:05144**	Malaria	1.42E-02
			KEGG:05418	Fluid shear stress and atherosclerosis	2.00E-02
			REAC:R-HSA-6785807	Interleukin-4 and Interleukin-13 signaling	7.15E-03
			REAC:R-HSA-449147	Signaling by Interleukins	1.37E-02
			REAC:R-HSA-6803207	TP53 Regulates Transcription of Caspase Activators and Caspases	4.74E-02

References

Acara AC, Bolatkale M, Kızıloğlu İ, İbişoğlu E & Can Ç (2018) A novel biochemical marker for predicting the severity of ACS with unstable angina pectoris: Asprosin. *Am J Emerg Med* 36: 1504–1505 doi: 10.1016/j.ajem.2017.12.032 [PREPRINT]

Adapala VJ, Ward M & Ajuwon KM (2012) Adipose tissue biglycan as a potential anti-inflammatory target of sodium salicylate in mice fed a high fat diet. *J Inflamm (United Kingdom)* 9: 1–7

Alessi MC & Juhan-Vague I (2006) PAI-1 and the metabolic syndrome: Links, causes, and consequences. *Arterioscler Thromb Vasc Biol* 26: 2200–2207

Antonopoulos AS, Sanna F, Sabharwal N, Thomas S, Oikonomou EK, Herdman L, Margaritis M, Shirodaria C, Kampoli AM, Akoumianakis I, *et al* (2017) Detecting human coronary inflammation by imaging perivascular fat. *Sci Transl Med* 9

Aroor AR, Jia G & Sowers JR (2018) Cellular mechanisms underlying obesity-induced arterial stiffness. *Am J Physiol Regul Integr Comp Physiol* 314: R387–R398

Bayes-Genis A, Conover CA, Overgaard MT, Bailey KR, Christiansen M, Holmes DRJ, Virmani R, Oxvig C & Schwartz RS (2001) Pregnancy-associated plasma protein A as a marker of acute coronary syndromes. *N Engl J Med* 345: 1022–1029

Berg AH & Scherer PE (2005) Adipose tissue, inflammation, and cardiovascular disease. *Circ Res* 96: 939–949

Berti L, Hartwig S, Irmler M, Rädle B, Siegel-Axel D, Beckers J, Lehr S, Al-Hasani H, Häring H-U, Hrabě de Angelis M, *et al* (2016) Impact of fibroblast growth factor 21 on the secretome of human perivascular preadipocytes and adipocytes: a targeted proteomics approach. *Arch Physiol Biochem* 122: 281–288

Britton KA, Massaro JM, Murabito JM, Kreger BE, Hoffmann U & Fox CS (2013) Body fat distribution, incident cardiovascular disease, cancer, and all-cause mortality. *J Am Coll Cardiol* 62: 921–925

Browaeys R, Saelens W & Saeys Y (2020) NicheNet: modeling intercellular communication by linking ligands to target genes. *Nat Methods* 17: 159–162

Buechler C, Krautbauer S & Eisinger K (2015) Adipose tissue fibrosis. *World J Diabetes* 6: 548

Byon CH, Han T, Wu J & Hui ST (2015) Txnip ablation reduces vascular smooth muscle cell inflammation and ameliorates atherosclerosis in apolipoprotein E knockout mice. *Atherosclerosis* 241: 313–321

Carroll JF & Tyagi SC (2005) Extracellular Matrix Remodeling in the Heart of the Homocysteinemic Obese Rabbit. *Am J Hypertens* 18: 692–698

Chatterjee TK, Aronow BJ, Tong WS, Manka D, Tang Y, Bogdanov VY, Unruh D, Blomkalns AL, Piegore MGJ, Weintraub DS, *et al* (2013) Human coronary artery perivascular adipocytes overexpress genes responsible for regulating vascular morphology, inflammation, and hemostasis. *Physiol Genomics* 45: 697–709

Choe SS, Huh JY, Hwang IJ, Kim JI & Kim JB (2016) Adipose Tissue Remodeling: Its Role in Energy Metabolism and Metabolic Disorders. *Front Endocrinol (Lausanne)* 7: 30

Chun T-H (2012) Peri-adipocyte ECM remodeling in obesity and adipose tissue fibrosis. *Adipocyte* 1: 89–95

Conover CA, Harstad SL, Tchkonia T & Kirkland JL (2013) Preferential impact of pregnancy-associated plasma protein-A deficiency on visceral fat in mice on high-fat diet. *Am J Physiol Endocrinol Metab* 305: E1145-53

Corvera S & Gealekman O (2014) Adipose tissue angiogenesis: impact on obesity and type-2 diabetes. *Biochim Biophys Acta* 1842: 463–472

Cushing EM, Chi X, Sylvers KL, Shetty SK, Potthoff MJ & Davies BSJ (2017) Angiopoietin-like 4 directs uptake of dietary fat away from adipose during fasting. *Mol Metab* 6: 809–818

Datta R, Podolsky MJ & Atabai K (2018) Fat fibrosis: friend or foe? *JCI insight* 3

Davis MR, Arner E, Duffy CRE, De Sousa PA, Dahlman I, Arner P & Summers KM (2016) Expression of FBN1 during adipogenesis: Relevance to the lipodystrophy phenotype in Marfan syndrome and related conditions. *Mol Genet Metab* 119: 174–185

Divoux A & Clément K (2011) Architecture and the extracellular matrix: the still unappreciated components of the adipose tissue. *Obes Rev an Off J Int Assoc Study Obes* 12: e494-503

Eriksson AKS, van Harmelen V, Stenson BM, Aström G, Wåhlén K, Laurencikiene J & Rydén M (2009) Endothelin-1 stimulates human adipocyte lipolysis through the ET A receptor. *Int J Obes (Lond)* 33: 67–74

Ewels PA, Peltzer A, Fillinger S, Patel H, Alneberg J, Wilm A, Garcia MU, Di Tommaso P & Nahnsen S (2020) The nf-core framework for community-curated bioinformatics pipelines. *Nat Biotechnol* 38: 276–278 doi:10.1038/s41587-020-0439-x [PREPRINT]

Galis ZS & Khatri JJ (2002) Matrix metalloproteinases in vascular remodeling and atherogenesis: the good, the bad, and the ugly. *Circ Res* 90: 251–262

Gao D & Bing C (2011) Macrophage-induced expression and release of matrix metalloproteinase 1 and 3 by human preadipocytes is mediated by IL-1β via activation of MAPK signaling. *J Cell Physiol* 226: 2869–2880

Goossens GH, Blaak EE, Saris WHM & van Baak MA (2004) Angiotensin II-induced effects on adipose and skeletal muscle tissue blood flow and lipolysis in normal-weight and obese subjects. *J Clin Endocrinol Metab* 89: 2690–2696

Gustafson B & Smith U (2006) Cytokines promote Wnt signaling and inflammation and impair the normal differentiation and lipid accumulation in 3T3-L1 preadipocytes. *J Biol Chem* 281: 9507–9516

Guzik TJ, Skiba DS, Touyz RM & Harrison DG (2017) The role of infiltrating immune cells in dysfunctional adipose tissue. *Cardiovasc Res* 113: 1009–1023

Ha EE & Bauer RC (2018) Emerging Roles for Adipose Tissue in Cardiovascular Disease. *Arterioscler Thromb Vasc Biol* 38: e137–e144

Halberg N, Khan T, Trujillo ME, Wernstedt-Asterholm I, Attie AD, Sherwani S, Wang Z V, Landskroner-Eiger S, Dineen S, Magalang UJ, *et al* (2009) Hypoxia-inducible factor 1alpha induces fibrosis and insulin resistance in white adipose tissue. *Mol Cell Biol* 29: 4467–4483

Han H (2018) RNA Interference to Knock Down Gene Expression. *Methods Mol Biol* 1706: 293–302

Heeneman S, Cleutjens JP, Faber BC, Creemers EE, van Suylen R-J, Lutgens E, Cleutjens KB & Daemen MJ (2003) The dynamic extracellular matrix: intervention strategies during heart failure and atherosclerosis. *J Pathol* 200: 516–525

Henegar C, Tordjman J, Achard V, Lacasa D, Cremer I, Guerre-Millo M, Poitou C, Basdevant A, Stich V, Viguerie N, *et al* (2008) Adipose tissue transcriptomic signature highlights the pathological relevance of extracellular matrix in human obesity. *Genome Biol* 9: R14

Howson JMM, Zhao W, Barnes DR, Ho W-K, Young R, Paul DS, Waite LL, Freitag DF, Fauman EB, Salfati EL, *et al* (2017) Fifteen new risk loci for coronary artery disease highlight arterial-wall-specific mechanisms. *Nat Genet* 49: 1113–1119

Katsuda S & Kaji T (2003) Atherosclerosis and extracellular matrix. *J Atheroscler Thromb* 10: 267–274

Kaur P, Reis MD, Couchman GR, Forjuoh SN, Greene JF & Asea A (2010) SERPINE 1 Links Obesity and Diabetes: A Pilot Study. *J Proteomics Bioinform* 3: 191–199

Keophiphath M, Achard V, Henegar C, Rouault C, Clément K & Lacasa D (2009) Macrophage-secreted factors promote a profibrotic phenotype in human preadipocytes. *Mol Endocrinol* 23: 11–24

Khachigian LM (2006) Early growth response-1 in cardiovascular pathobiology. *Circ Res* 98: 186–191

Kong P, Gonzalez-Quesada C, Li N, Cavalera M, Lee D-W & Frangogiannis NG (2013) Thrombospondin-1 regulates adiposity and metabolic dysfunction in diet-induced obesity enhancing adipose inflammation and stimulating adipocyte proliferation. *Am J Physiol Metab* 305: E439–E450

Lee SH, Park HS, Lee JA, Song YS, Jang YJ, Kim J-H, Lee YJ & Heo Y (2013) Fibronectin gene expression in human adipose tissue and its associations with obesity-related genes and metabolic parameters. *Obes Surg* 23: 554–560

León-Pedroza JI, González-Tapia LA, del Olmo-Gil E, Castellanos-Rodríguez D, Escobedo G & González-Chávez A (2015) Low-grade systemic inflammation and the development of metabolic diseases: from the molecular evidence to the clinical practice. *Cir Cir* 83: 543–551

Lessard J, Pelletier M, Biertho L, Biron S, Marceau S, Hould F-S, Lebel S, Moustarah F, Lescelleur O, Marceau P, *et al* (2015) Characterization of dedifferentiating human mature adipocytes from the visceral and subcutaneous fat compartments: fibroblast-activation protein alpha and dipeptidyl peptidase 4 as major components of matrix remodeling. *PLoS One* 10: e0122065

Liang X, Kanjanabuch T, Mao S-L, Hao C-M, Tang Y-W, Declerck PJ, Hasty AH, Wasserman DH, Fogo AB & Ma L-J (2006) Plasminogen activator inhibitor-1 modulates adipocyte differentiation. *Am J Physiol Metab* 290: E103–E113

Libby P, Ridker PM & Maseri A (2002) Inflammation and atherosclerosis. *Circulation* 105: 1135–1143

Lim S & Meigs JB (2014) Links between ectopic fat and vascular disease in humans. *Arterioscler Thromb Vasc Biol* 34: 1820–1826

Lin D, Chun T-H & Kang L (2016) Adipose extracellular matrix remodelling in obesity and insulin resistance. *Biochem Pharmacol* 119: 8–16

Liu LF, Kodama K, Wei K, Tolentino LL, Choi O, Engleman EG, Butte AJ & McLaughlin T (2015) The receptor CD44 is associated with systemic insulin resistance and proinflammatory macrophages in human adipose tissue. *Diabetologia* 58: 1579–1586

Livak KJ & Schmittgen TD (2001) Analysis of relative gene expression data using real-time quantitative PCR and the 2(-Delta Delta C(T)) Method. *Methods* 25: 402–408

Love MI, Huber W & Anders S (2014) Moderated estimation of fold change and dispersion for RNA-seq data with DESeq2. *Genome Biol* 15: 550

Marcelin G, Ferreira A, Liu Y, Atlan M, Aron-Wisnewsky J, Pelloux V, Botbol Y, Ambrosini M, Fradet M, Rouault C, *et al* (2017) A PDGFRα-Mediated Switch toward CD9(high) Adipocyte Progenitors Controls Obesity-Induced Adipose Tissue Fibrosis. *Cell Metab* 25: 673–685

Martin M (2011) Cutadapt removes adapter sequences from high-throughput sequencing reads. *EMBnet.journal* 17: 10–12, doi: 10.14806/ej.17.1.200

Mathew V, Hasdai D & Lerman A (1996) The role of endothelin in coronary atherosclerosis. *Mayo Clin Proc* 71: 769–777

Matsui Y, Rittling SR, Okamoto H, Inobe M, Jia N, Shimizu T, Akino M, Sugawara T, Morimoto J, Kimura C, *et al* (2003) Osteopontin deficiency attenuates atherosclerosis in female apolipoprotein E-deficient mice. *Arterioscler Thromb Vasc Biol* 23: 1029–1034

Moura R, Tjwa M, Vandervoort P, Van Kerckhoven S, Holvoet P & Hoylaerts MF (2008) Thrombospondin-1 deficiency accelerates atherosclerotic plaque maturation in ApoE-/- mice. *Circ Res* 103: 1181–1189

Muthu ML & Reinhardt DP (2020) Fibrillin-1 and fibrillin-1-derived asprosin in adipose tissue function and metabolic disorders. *J Cell Commun Signal* 14: 159–173

Napolitano L (1963) The differentiation of white adipose cells. An electron microscope study. *J Cell Biol* 18: 663–679

Nie J & Sage EH (2009) SPARC inhibits adipogenesis by its enhancement of beta-catenin signaling. *J Biol Chem* 284: 1279–1290

Ohman MK, Shen Y, Obimba CI, Wright AP, Warnock M, Lawrence DA & Eitzman DT (2008) Visceral adipose tissue inflammation accelerates atherosclerosis in apolipoprotein E-deficient mice. *Circulation* 117: 798–805

Oikonomou EK & Antoniades C (2019) The role of adipose tissue in cardiovascular health and disease. *Nat Rev Cardiol* 16: 83–99

Ouwens DM, Sell H, Greulich S & Eckel J (2010) The role of epicardial and perivascular adipose tissue in the pathophysiology of cardiovascular disease. *J Cell Mol Med* 14: 2223–2234

Parvizi M, Ryan ZC, Ebtehaj S, Arendt BK & Lanza IR (2021) The secretome of senescent preadipocytes influences the phenotype and function of cells of the vascular wall. *Biochim Biophys acta Mol basis Dis* 1867: 165983

Raajendiran A, Ooi G, Bayliss J, O'Brien PE, Schittenhelm RB, Clark AK, Taylor RA, Rodeheffer MS, Burton PR & Watt MJ (2019) Identification of Metabolically Distinct Adipocyte Progenitor Cells in Human Adipose Tissues. *Cell Rep* 27: 1528-1540.e7

Riessen R, Isner JM, Blessing E, Loushin C, Nikol S & Wight TN (1994) Regional differences in the distribution of the proteoglycans biglycan and decorin in the extracellular matrix of atherosclerotic and restenotic human coronary arteries. *Am J Pathol* 144: 962–974

Rittig K, Dolderer JH, Balletshofer B, Machann J, Schick F, Meile T, Küper M, Stock UA, Staiger H, Machicao F, *et al* (2012) The secretion pattern of perivascular fat cells is different from that of subcutaneous and visceral fat cells. *Diabetologia* 55: 1514–1525

Roberts AB, McCune BK & Sporn MB (1992) TGF-beta: regulation of extracellular matrix. *Kidney Int* 41: 557–559

Robinson MD, McCarthy DJ & Smyth GK (2010) edgeR: a Bioconductor package for differential expression analysis of digital gene expression data. *Bioinformatics* 26: 139–140

Ruiz-Ojeda FJ, Méndez-Gutiérrez A, Aguilera CM & Plaza-Díaz J (2019) Extracellular Matrix Remodeling of Adipose Tissue in Obesity and Metabolic Diseases. *Int J Mol Sci* 20

Ruiz-Ojeda FJ, Wang J, Bäcker T, Krueger M, Zamani S, Rosowski S, Gruber T, Onogi Y, Feuchtinger A, Schulz TJ, *et al* (2021) Active integrins regulate white adipose tissue insulin sensitivity and brown fat thermogenesis. *Mol Metab* 45: 101147

Sadanandam A, Rosenbaugh EG, Singh S, Varney M & Singh RK (2010) Semaphorin 5A promotes angiogenesis by increasing endothelial cell proliferation, migration, and decreasing apoptosis. *Microvasc Res* 79: 1–9

Sartore S, Chiavegato A, Faggin E, Franch R, Puato M, Ausoni S & Pauletto P (2001) Contribution of adventitial fibroblasts to neointima formation and vascular remodeling: from innocent bystander to active participant. *Circ Res* 89: 1111–1121

Schneiderman J, Sawdey MS, Keeton MR, Bordin GM, Bernstein EF, Dilley RB & Loskutoff DJ (1992) Increased type 1 plasminogen activator inhibitor gene expression in atherosclerotic human arteries. *Proc Natl Acad Sci U S A* 89: 6998–7002

Strieder-Barboza C, Baker NA, Flesher CG, Karmakar M, Neeley CK, Polsinelli D, Dimick JB, Finks JF, Ghaferi AA, Varban OA, *et al* (2019) Advanced glycation end-products regulate extracellular matrix-adipocyte metabolic crosstalk in diabetes. *Sci Rep* 9: 19748

Suganami T, Tanaka M & Ogawa Y (2012) Adipose tissue inflammation and ectopic lipid accumulation. *Endocr J* 59: 849–857

Sun K, Tordjman J, Clément K & Scherer PE (2013) Fibrosis and adipose tissue dysfunction. *Cell Metab* 18: 470–477

Takahashi M, Nagaretani H, Funahashi T, Nishizawa H, Maeda N, Kishida K, Kuriyama H, Shimomura I, Maeda K, Hotta K, *et al* (2001) The Expression of SPARC in Adipose Tissue and Its Increased Plasma Concentration in Patients with Coronary Artery Disease. *Obes Res* 9: 388–393

Thorin E & Webb DJ (2013) Endothelium-derived endothelin-1. 459: 951–958

Trivedi CM, Patel RC & Patel C V (2007) Homeobox gene HOXA9 inhibits nuclear factor-kappa B dependent activation of endothelium. *Atherosclerosis* 195: e50-60

Ueno H, Koyama H, Shoji T, Monden M, Fukumoto S, Tanaka S, Otsuka Y, Mima Y, Morioka T, Mori K, *et al* (2010) Receptor for advanced glycation end-products (RAGE) regulation of adiposity and adiponectin is associated with atherogenesis in apoE-deficient mouse. *Atherosclerosis* 211: 431–436

Vacek TP, Rehman S, Neamtu D, Yu S, Givimani S & Tyagi SC (2015) Matrix metalloproteinases in atherosclerosis: role of nitric oxide, hydrogen sulfide, homocysteine, and polymorphisms. *Vasc Health Risk Manag* 11: 173–183

van der Harst P & Verweij N (2018) Identification of 64 Novel Genetic Loci Provides an Expanded View on the Genetic Architecture of Coronary Artery Disease. *Circ Res* 122: 433–443

Wabitsch M, Brenner RE, Melzner I, Braun M, Möller P, Heinze E, Debatin KM & Hauner H (2001) Characterization of a human preadipocyte cell strain with high capacity for adipose differentiation. *Int J Obes Relat Metab Disord J Int Assoc Study Obes* 25: 8–15

Ward M & Ajuwon KM (2011) Regulation of pre-adipocyte proliferation and apoptosis by the small leucine-rich proteoglycans, biglycan and decorin. *Cell Prolif* 44: 343–351

Yin C, Xiao Y, Zhang W, Xu E, Liu W, Yi X & Chang M (2014) DNA microarray analysis of genes differentially expressed in adipocyte differentiation. *J Biosci* 39: 415–423

Yoshino J, Patterson BW & Klein S (2019) Adipose Tissue CTGF Expression is Associated with Adiposity and Insulin Resistance in Humans. *Obesity (Silver Spring)* 27: 957–962

Yue B (2014) Biology of the extracellular matrix: an overview. *J Glaucoma* 23: S20-3

Zhang J, Zhang Y, Sun T, Guo F, Huang S, Chandalia M, Abate N, Fan D, Xin H-B, Chen YE, *et al* (2013) Dietary obesity-induced Egr-1 in adipocytes facilitates energy storage via suppression of FOXC2. *Sci Rep* 3: 1476

Zheng Q, Ma Y, Chen S, Che Q & Chen D (2020) The Integrated Landscape of Biological Candidate Causal Genes in Coronary Artery Disease. *Front Genet* 11: 320

Zorena K, Jachimowicz-Duda O, Ślęzak D, Robakowska M & Mrugacz M (2020) Adipokines and Obesity. Potential Link to Metabolic Disorders and Chronic Complications. *Int J Mol Sci* 21